The mean state and variability of the North Atlantic circulation: a perspective from ocean reanalyses

Article

Accepted Version

The mean state and variability of the North Atlantic circulation: a perspective from ocean reanalyses

L C Jackson[1], C Dubois[2,3], G Forget[4], K Haines[5], M Harrison[6], D Iovino[7], A Köhl[8], D Mignac[9], S Masina[7], K A Peterson[1,10], C G Piecuch[11], C Roberts[12], J Robson[13], A Storto[7,14], T Toyoda[15], M Valdivieso[9], C Wilson[16], Y Wang[17], H Zuo[12]

[1]Met Office Hadley Centre, UK
[2]Mercator Ocean International, France
[3]Météo France, France
[4]MIT, USA
[5]Department of Meteorology and National Centre for Earth Observation, University of Reading, UK
[6]GFDL, USA
[7]Foundation Euro-Mediterranean Centre on Climate Change, Italy
[8]Institute of Oceanography, University of Hamburg, Germany
[9]Department of Meteorology, University of Reading, UK
[10]Environmental Numerical Research Section, Environment and Climate Change Canada, Canada
[11]Woods Hole Oceanographic Institution, USA
[12]The European Centre for Medium-Range Weather Forecasts, UK
[13]National Centre for Atmospheric Science, Department of Meteorology, University of Reading, UK
[14]NATO STO Centre for Maritime Research and Experimentation, Italy
[15]Meteorological Research Institute, Japan Meteorological Agency, Japan
[16]National Oceanography Centre, Liverpool, UK
[17]Nansen Environmental and Remote Sensing Centre/Bjerknes Center for Climate Research, Norway

Key Points:

- Ocean reanalyses are potentially useful tools for understanding ocean circulation.
- Some consistency among reanalyses in interannual and decadal variability of the circulation.
- Improvements in some aspects of the ocean circulation as the observational coverage has improved.

Corresponding author: Laura Jackson, laura.jackson@metoffice.gov.uk

Abstract

The observational network around the North Atlantic has improved significantly over the last few decades with subsurface profiling floats and satellite observations, and the recent efforts to monitor the Atlantic Meridional Overturning Circulation (AMOC). These have shown decadal timescale changes across the North Atlantic including in heat content, heat transport and the circulation. However there are still significant gaps in the observational coverage. Ocean reanalyses integrate the observations with a dynamically consistent ocean model and can be used to understand the observed changes. However the ability of the reanalyses to represent the dynamics must also be assessed.

We use an ensemble of global ocean reanalyses to examine the time mean state and interannual-decadal variability of the North Atlantic ocean since 1993. We assess how well the reanalyses are able to capture processes and whether any understanding can be gained. In particular we examine aspects of the circulation including convection, AMOC and gyre strengths, and transports. We find that reanalyses show some consistency, in particular showing a weakening of the subpolar gyre and AMOC at 50^oN from the mid-90s until at least 2009 (related to decadal variability in previous studies), a strengthening and then weakening of the AMOC at 26.5^oN since 2000, and impacts of circulation changes on transports. These results agree with model studies and the AMOC observations at 26.5^oN since 2005. We also see less spread across the ensemble in AMOC strength and mixed layer depth, suggesting improvements as the observational coverage has improved.

Plain language summary

The observational network around the North Atlantic has improved significantly over the last few decades revealing changes over decadal timescales in the North Atlantic, including in heat content, heat transport and the circulation. However there are still significant gaps in the observational coverage. Ocean reanalyses fill in these gaps by combining the observations with a computer model of the ocean to give consistent estimates of the ocean state. These reanalyses are potentially useful tools that can be used to understand the observed changes, however their skill must also be assessed.

We use an ensemble of global ocean reanalyses in order to examine the mean state and variability of the North Atlantic ocean since 1993. In particular we examine the con-

vection, the circulation, transports of heat and fresh water and temperature and salinity changes. We find that reanalyses show some consistency in their results, suggesting that they may be useful for understanding circulation changes in regions and times where there are no observations. We also show improvements in some aspects of the ocean circulation as the observational coverage has improved. This highlights the importance of continuing observational campaigns.

1 Introduction

Although the North Atlantic has warmed since preindustrial times (Collins et al., 2013), it has also exhibited large variability on different timescales, particularly of upper ocean temperatures (Sutton et al., 2018; Knight et al., 2005). This variability has been shown to have wide-ranging impacts, for instance on precipitation in Europe (Sutton & Dong, 2012), the North Atlantic storm track (Peings & Magnusdottir, 2014), monsoons, and hurricane frequency (R. Zhang & Delworth, 2006; Smith et al., 2010). As well as decadal and multi-decadal variability, there has also been significant interannual variability, such as significant cooling of the subtropics in 2010 and the recent cooling of the subpolar gyre (Cunningham et al., 2013; Grist et al., 2016). These sea surface temperature anomalies can influence the weather and climate over Europe (Josey et al., 2018), in particular through influencing the winter North Atlantic Oscillation (Cassou et al., 2007), summer precipitation (Dunstone et al., 2018) and potentially heat waves (Duchez et al., 2016). Increasing observational coverage over the last few decades, particularly with satellite measurements of sea level and sea surface temperatures (SST), and the Argo network providing temperature and salinity profiles, has revealed large changes in ocean properties and generated a need to understand the processes driving the changes (Robson et al., 2018; von Schuckmann & et al, 2018).

In the subpolar gyre a warming was observed in the late 1990s, and several model-based studies have now attributed this warming to increased northwards heat transport due to a strong Atlantic Meridional Overturning Circulation (AMOC) (Robson et al., 2012; Williams et al., 2014; Yeager & Danabasoglu, 2014), while some reanalysis studies (Yang et al., 2016; Piecuch et al., 2017) suggest that changes in gyre advection were important as well. Although we do not have direct measurements of the strength of the AMOC during this period, model experiments generally agree that the AMOC in the subpolar region was strong in the mid 90s and weakened over the following decade (Robson

et al., 2012; Danabasoglu et al., 2016). Similarly the subpolar gyre (SPG) strength was found to be strong in the mid 90s and then weakened, in agreement with proxies for SPG strength based on altimeter data (Häkkinen & Rhines, 2004). Studies have linked the strong AMOC and SPG circulations in the mid 1990s to increased densities in the Labrador Seas caused by buoyancy forcing during a persistently positive phase of the North Atlantic Oscillation (NAO) in the preceding years (Eden & Willebrand, 2001; Deshayes & Frankignoul, 2008; Lohmann et al., 2009; Robson et al., 2012; Yeager & Danabasoglu, 2014; Yang et al., 2016). However recent observations have suggested that the AMOC could be more influenced by water mass transformations to the east of Greenland (Lozier et al., 2019). More recently the warming and salinification of the subpolar region has reversed to a cooling and freshening, consistent with weakening heat and salt transports (Robson et al., 2016; Hermanson et al., 2014), although there is also strong evidence that the more extreme cooling seen in 2014 was caused by anomalous surface heat fluxes (Grist et al., 2016; Josey et al., 2018). This cooling has resulted in an increase in density in the Labrador Seas, with an associated increase in deep convection (Yashayaev & Loder, 2017).

In the subtropics the variability has been markedly different with interannual variability superimposed on a more gradual warming trend (Robson et al., 2018; Williams et al., 2014). The AMOC at 26.5^oN has been monitored since 2004 by the RAPID-MOCHA array (McCarthy et al., 2015) revealing interannual variability including a large, temporary weakening in winter 2009-2010, believed to be wind-driven (McCarthy et al., 2012; C. D. Roberts et al., 2013a; Evans et al., 2017) that caused a cooling of the subtropics (Cunningham et al., 2013). The AMOC strength has also weakened since 2004, and has been found to be in a weaker state since 2008 (Smeed et al., 2018). Although there have been suggestions of a longer term (centennial) weakening (Caesar et al., 2018; Thornalley et al., 2018), there is some evidence that the observed decadal weakening is due to decadal variability (Jackson et al., 2016). Prior to 2004 there were only intermittent measurements of AMOC strength. Although modeling studies mostly agree that the AMOC in the subpolar gyre was strong in the mid 90s and then weakened, there is more disagreement amongst models about the changes in the subtropical gyre (Danabasoglu et al., 2016). Jackson et al. (2016), using an ocean reanalysis that agreed well with the RAPID observations, suggested that the AMOC at 26.5^oN increased over the decade up to 2004 and then weakened after as a lagged response to the weakening of the subpolar AMOC and Labrador Sea densities during the previous decade. Previous model-based studies

have also shown a lagged relationship between the subpolar and subtropical AMOC (Yeager & Danabasoglu, 2014), and a relationship of the AMOC with densities in the Labrador Sea (Robson et al., 2014).

A greater understanding of these processes can help to separate natural variability from anthropogenic change. It is also fundamental to our ability to make predictions on interannual to centennial timescales. However observations are still limited, particularly when it comes to transports and process-related quantities such as convection. Ocean and climate models are useful tools in studying such processes, however they suffer from biases and can show a wide range of timescales and driving processes of variability. One tool that has been less used so far is the ocean reanalysis. Reanalyses are ocean models that are forced by meteorological boundary conditions from atmospheric reanalyses and assimilate observations such as in situ temperature and salinity, SST, sea level anomalies and sea ice concentration (Storto et al., 2019). As such, they integrate the observations within a dynamically consistent ocean model, although the assimilation itself can alter the dynamics. Reanalyses differ with regard to the types of observations assimilated, the method of assimilation, the surface forcing, and of course the ocean model used (Balmaseda et al., 2015), with those designed to cover the satellite period able to use more observational types than those covering longer periods. An advantage of reanalyses as compared to other data products is that they can provide transports, and other properties, that can be hard to measure continuously. However care must be taken that the reanalysis is sufficiently constrained by the observations in the region of interest, and that the constraints themselves do not adversely affect the processes involved creating spurious results (Storto et al., 2019). Multimodel ensembles can help interpretation by providing a range of possible behaviors (Masina et al., 2017; Storto et al., 2018). There is also temporal variability in the type and number of observations assimilated, so users must be aware that the quality of the reanalysis for a particular purpose could change in time.

The ORA (Ocean Reanalysis) Intercomparison Project was initiated under CLIVAR GSOP and GODAE-Oceanview and has produced a series of papers examining global ocean reanalyses and focusing on different aspects of the ocean state (e.g. steric sea level, air-sea fluxes, ocean heat and salt content among others). These were then brought together in a special issue of Climate Dynamics (Balmaseda et al., 2015; Toyoda et al., 2017a, 2017b; Chevallier et al., 2017; Tietsche et al., 2017; Karspeck et al., 2017; Shi et al., 2017;

Valdivieso et al., 2017; Palmer et al., 2017; Masina et al., 2017; Storto et al., 2017). A further paper on the polar oceans was later added (Uotila et al., 2018). Most of these papers focused on consistency of the mean states amongst reanalyses although several also looked at diagnostics of variability. Palmer et al. (2017) showed many reanalyses had consistent ocean heat content (OHC) trends as a function of depth, and that a significant component of recent OHC increase was below 700m depth. The North Atlantic was seen to be an area of substantial agreement in upper OHC trends, consistent with this being a better observed region. However there have been substantial disagreements shown across reanalyses: Karspeck et al. (2017) looked at the AMOC in long reanalyses starting before 1960, and found disagreement in AMOC variability and strength in these early, observation-sparse periods.

This study advances beyond many previous ORA studies in presenting a more process oriented approach aimed at understanding differences and similarities. We focus on the dynamics of the North Atlantic since 1993, which is when satellite altimetry data (e.g. see Forget and Ponte (2015)) became routinely available and vastly increased the observations that could be assimilated in a reanalysis. Over this period the increase in observations has also revealed changes in temperature and salinity in the North Atlantic, along with changes in circulation patterns both observed and inferred. The aim of this study is to examine the climatology and inter-annual to decadal changes of the North Atlantic ocean in a multi-model ensemble of global ocean reanalyses. In particular we ask: Where is there agreement or disagreement across reanalyses? Can we learn what makes reanalyses good at specific processes? Can these reanalyses improve our understanding of the dynamics in the North Atlantic ocean?

Section 2 describes the reanalyses used. We then discuss the climatologies of the products in section 3 and the changes seen in section 4. Section 5 provides a discussion and summary. We also list acronyms used in Table 1.

2 Models and methods

2.1 Reanalyses

In this study, we have analyzed data from eleven ORA products (C-GLORSv7, ECCO V4 R3, ECDA3, GECCO2, GLORYS2v4, GLORYS12v1, GloSea5, GONDOLA100A, NorCPM-v1, ORAS5 and UR025.4) in the North Atlantic (Table 2). It should also be noted that

6 of the reanalyses use the NEMO ocean model and 5 of these use the same resolution (0.25^o). The latest addition to this set of NEMO reanalyses is the higher resolution ($1/12^o$) GLORYS12v1 reanalysis that has been included in this study. Although these reanalyses use very similar models and assimilated data, they do differ in the assimilation techniques used, and there are still many interesting differences in the results (Storto et al., 2018). The other products however cover a wide range of model systems, resolutions, and data assimilation approaches. ECCO V4 R3 and GECCO2 use a 4DVar assimilation scheme which optimizes the solution through adjusting parameters (including surface fluxes, wind stresses, mixing parameters) rather than apply increments in temperature and salinity. The NorCPM-v1 reanalysis has a coupled atmospheric component and hence has quite different surface fluxes and wind stresses from the other reanalyses, which are forced by atmospheric reanalysis fields. In NorCPM-v1 there is no atmospheric constraint and assimilation is only carried on the ocean component (weakly coupled data assimilation). The adjustment in the other components (atmosphere, sea ice) occurs dynamically during the integration of the system. NorCPM-v1 is also an outlier in being the only reanalysis using anomaly rather than full field assimilation, hence its mean state is unconstrained by observations. We do include it in the analysis for completeness.

2.2 Observational data

Where appropriate we also compare the ensemble to observational estimates, although in some circumstances suitable observational estimates are not available. We include temperatures, salinities and densities from the gridded observational analyses EN4 (Good et al., 2013) and CORA (Cabanes et al., 2013). These use some of the same data as assimilated in the reanalyses (in particular subsurface temperature and salinity profiles), however they use statistical techniques to infill missing data, rather than assimilation in a dynamical model. We also include AMOC volume and heat transports from the RAPID-MOCHA array (McCarthy et al., 2015; Smeed et al., 2017; Johns et al., 2011), volume transports from the new OSNAP array (Lozier et al., 2019) and various estimates of the meridional heat and freshwater transports from sections across the North Atlantic. We also include a comparison with the climatological estimate of the March mixed layer depth from de Boyer-Montegut, Madec, Fischer, Lazar, and Iudicone (2004).

2.3 Methods

Definitions of individual diagnostics are included in the sections and figure captions. Not all data were made available from all reanalyses, hence not all reanalyses are included in all figures.

We use climatologies based on the years 1993-2010 since that is the common period available for all reanalyses, apart from mixed layer depths where we use a more recent period (2004-2010) since there is large uncertainty earlier than that. Timeseries are shown for the full period (since 1993) for each reanalysis, some of which extend to 2017. For timeseries we use monthly means where available (some diagnostics were only available as annual means for NorCPM-v1). We examine interannual to decadal changes by smoothing monthly values with a 12 month running mean, which also has the advantage of removing the seasonal cycle. Timeseries are shown as either the total value (with smoothing) or as anomalies from the climatology of the relevant reanalysis.

Significance of relationships between two variables are tested using a null hypothesis that there is no correlation or no trend and a 95% confidence interval (p=0.05). Correlation coefficients (R) and probabilities of the null test (p) are quoted. In particular the correlations of scatter plots between two variables or between two timeseries are tested using a t test (with the null hypothesis that there is no correlation). Significance of a trend in a timeseries is tested against the variability of that timeseries (using a t test and the null hypothesis that the trend is zero). The significance of a difference between two n-year means is tested in comparison with the bootstrapped distribution of differences between n-year means.

3 Mean state

3.1 Convection and formation of deep water masses

March mixed layer depth climatologies are shown in Fig 1 (see caption for definition). These are often used as a proxy for deep convection, which alters densities in the subpolar North Atlantic and hence affects ocean dynamics. There are two centres of deep convection in observations and reanalyses: in the Labrador and GIN (Greenland-Iceland-Norway) Seas. About half the reanalyses have depths of convection in the Labrador Seas that are comparable to the observational climatology (although this is based on a much longer time period, (de Boyer-Montegut et al., 2004)). The other half have too deep and

widespread convection, apart from GECCO2 where the mixed layer depth is very shallow. Most reanalyses have much too deep convection in the GIN seas, as has been noted in a previous reanalysis comparison (Uotila et al., 2018) and seen in coupled climate models (Heuzé, 2017). A previous comparison of mixed layer depths across reanalyses was also made by Toyoda et al. (2017a) who looked globally at shallow mixed layer depths, rather than regions of deep convection. They do note that there is little consistency amongst and between observational and reanalyses data sets at high latitudes.

3.2 Circulation

The AMOC streamfunction in many reanalyses looks similar to that found in free-running models (Danabasoglu et al., 2014), with a North Atlantic overturning cell in the upper 3000m (Fig 2). This depicts the northwards volume transport in the upper 1000m of the Atlantic, followed by sinking and a southwards return flow between 1000-3000m approximately. In common with free-running models there are considerable differences in the latitude of the streamfunction maximum (Danabasoglu et al., 2016). In some cases there are discontinuities at some latitudes, possibly suggesting an impact of the assimilation scheme. In particular, GloSea5 is suspect in the South Atlantic and near the equator (where there is a discontinuity in streamfunction strength): this issue has been traced to the method of assimilating sea surface height, and will be the subject of a future publication (M. Bell, personal communication). In most reanalyses the reversed Antarctic Bottom Water cell below 3000m is very weak compared to forced and coupled models (Ba et al., 2014; Danabasoglu et al., 2016). This could be because there is little constraint from data at these depths.

One place where the AMOC has been continuously monitored is at 26.5^oN, where the RAPID array (McCarthy et al., 2015) has been in place since 2004. Reanalysis profiles of the AMOC at this section (Fig 2, are calculated here using the same methodology as the observations (see C. D. Roberts et al. (2013a)) and for the same time period (2004-2010)). They show upper northwards transport (increasing streamfunction with depth) and deeper southwards transport (decreasing streamfunction). There is mostly a good agreement with the observations for the value and depth of the streamfunction maximum, although some reanalyses have too shallow a return flow. Previous studies have noted that data assimilation usually improves the AMOC mean strength over that

in forced ocean only models (Balmaseda et al., 2007; Tett et al., 2014; Karspeck et al., 2017).

Recently observations of the AMOC in the subpolar gyre have begun with the OSNAP initiative (Lozier et al., 2017). These have calculated an AMOC in density space with time mean profiles (Fig 13a) showing a northwards transport of Atlantic waters between densities 1027.2-1027.6 kg/m^3 and a denser return flow. There is also a small southwards transport of very light, surface waters. There is a good agreement with the magnitudes of the AMOC (14.9 $\pm$ 0.9 Sv) and the density at which the profile peaks in the observations (Lozier et al., 2019). Some reanalyses have a stronger overturning, however we note that the observational time series is short so far (<2 years), so the observational error on the long term mean is uncertain.

To assess the large-scale horizontal circulation we can compare the vertically integrated (barotropic) streamfunctions (Fig 3). These are the vertically integrated streamfunctions and are referenced to values on the eastern Atlantic coasts. They show two gyres: an anticyclonic subtropical gyre (STG) and cyclonic subpolar gyre (SPG), depicting the vertically integrated velocities. The medium (0.25^o) and high ($1/12^o$) resolution reanalyses clearly show more fine-scale features and a very localized intensification of the Gulf Stream near the western boundary, whereas lower resolution reanalyses have smoother subtropical gyres with generally broader boundary currents. This may be because of a greater influence of inertial recirculations at higher resolution, as previously found by Yeager (2015). Treguier, Deshayes, Lique, Dussin, and Molines (2012) also found that increased resolution strengthened the Gulf Stream.

To directly compare the circulations we split the STG and SPG into 4 boxes (Fig 4) covering the western boundary and interior regions. There is consistency between the interior gyre strength in the 6 NEMO models, and with ECCO V4 R3 and ECDA3. The outliers are NorCPM-v1 (which does not constrain the mean state) and GECCO2 where the interior STG is stronger than other reanalyses (see also subtropical gyre in Fig. 3). ECCO V4 R3 and GECCO2 use 4DVar which modifies surface fluxes within given error bounds, including wind stresses that have a strong impact on the gyre strengths through Sverdrup dynamics. Hence it is likely that modifications to wind stresses in GECCO2 have changed the gyre strengths, though we note that ECCO V4 R3 (which uses differ-

ent wind forcing products as the initial estimate and different optimization windows and iterations) has gyre strengths more consistent with other reanalyses.

In the interior of the subtropics the NorCPM-v1 and GONDOLA100A upper layer gyres are weaker (with smaller interior southward flow) but their gyres are deeper with perhaps 30% of the flow below 1100m, while most products have weaker deep interior southward flows. GECCO2 has a strong deep flow as well as a strong upper layer flow. We see no relationship between the depth of the interior flow and the depth of the AMOC circulation (Fig 2).

A comparison of the time mean strength of various circulation metrics is shown in Fig 5. There is a marginally significant relationship with reanalyses that have denser upper Labrador Sea (LS) densities having a stronger AMOC at 50^oN ($R = 0.60$, $p = 0.06$, Fig 5a). This is in agreement with results from an ocean only model intercomparison (Danabasoglu et al., 2014). Observational products (EN4 and CORA) show large uncertainties in the densities of the upper LS, however they suggest that those NEMO reanalyses with lighter upper LS and weaker AMOC at 50^oN (M50) are less realistic. There is no significant correlation between the AMOC at 26.5^oN (M26) and either M50 or the deeper Labrador Sea density (Fig 5b,c). Reanalyses with a stronger (more negative) SPG tend to have a weaker subpolar AMOC. This relationship is not significant ($R = 0.58$, $p = 0.13$, Fig 5d), though we note that the sample size is small. Danabasoglu et al. (2014) show a relationship between the AMOC strength and the Labrador Sea mixed layer depth (MLD), however we do not see such a relationship, possibly because the MLD is very noisy during the first part of the timeseries in many reanalyses (Fig 9c).

3.3 Transports

Time mean meridional ocean heat and freshwater transports (OHT/OFWT) are shown in Fig 6. These are calculated from monthly velocity, temperature and salinity fields and so do not include fluxes from variability at a higher frequency than monthly. Parameterized transports (Gent & McWilliams, 1990) are included for those reanalyses that use them. The OHT is northwards at every latitude through the Atlantic, with the maximum between 25 and 35 ^{o}N in most reanalyses. The OFWT has a minimum around 35-45^{o}N, showing a maximum in southwards freshwater transport. A reduction (increase)

in OFWT as latitude increase would be balanced in steady state by an export (import) of freshwater from surface fluxes.

Northwards heat transports (Fig 6a) at most latitudes are strongest in NorCPM-v1 (maximum 1.4 PW). It does not constrain the mean state and it is likely the transport is strong because of the strong AMOC (Fig 2). ECCO V4 R3 has the weakest heat transport at most latitudes with a maximum of 0.92 PW. Other reanalyses underestimate the transport around 26.5 ^{o}N, but mostly agree with the observational estimates further north of 35^{o}N. However it is possible that the methodology for the observational estimates at 26.5^{o}N could overestimate the heat transport (Stepanov et al., 2016). GloSea5 shows a rapid drop off of the heat transport in the South Atlantic caused by the very weak AMOC found there (Fig 2).

At 26.5^{o}N there is a significant correlation (R=0.79, p=0.02) of the mean AMOC strength with the total heat transport (Fig 7b), as seen across an ocean model ensemble (Danabasoglu et al., 2014). The heat and freshwater transport can also be decomposed into overturning and horizontal circulation components (and throughflow component for freshwater), see Bryden and Imawaki (2001); McDonagh et al. (2015). The relationship with the total heat content occurs because of a strong correlation of the AMOC with the overturning heat transport at 26.5^{o}N (R=0.81, p=0.01, Fig 7a). However using this relationship to predict observed heat transports from AMOC strength, underestimates the observed heat transport (Johns et al., 2011), even when comparing with the reanalyses available over the RAPID climatology period (2005-2015). This discrepancy has been seen in many models previously (Danabasoglu et al., 2014) and in previous reanalyses (Masina et al., 2017). Msadek et al. (2013) attribute this to an underestimation of the gyre component (due to poor representation of the transports near the western boundary) and an underestimation of the overturning part because of an overly diffusive thermocline. Figure 16 shows that most reanalyses underestimate both of these components.

Further north (50^{o}N), the AMOC still determines the overturning part of the heat transport, however the gyre transport is important as well (Fig 17). It should be noted that the decomposition into gyre and overturning components in the subpolar North Atlantic is less meaningful than in the subtropics since the thermohaline circulation projects onto both components. We can look at the relationships with the total heat transport,

but find no significant relationship between the total heat transport and either the SPG or M50 strength (Fig 7f,h).

For freshwater transport (Fig 6b), all reanalyses transport freshwater southwards across the equator due to the horizontal circulation, (see (Mignac et al., 2019)), other than NorCPM-v1 which is fully coupled and the atmospheric bias is a main contributor to the ocean bias in the tropical Atlantic (Lübbecke et al., 2018). The NEMO reanalyses all show relatively strong southward transport at 36, 45 and 53^{o}N. They also show greater transports of heat than the other reanalyses between 30 and 55^{o}N, and this may be because of their eddy-permitting resolution since ocean models have been shown to have differences in heat and fresh water transport with resolution (Treguier et al., 2012; M. J. Roberts et al., 2016). Observational estimates at 36^{o}N show a wide range of values and do not constrain the reanalyses.

There is a significant relationship (R=-0.84, p=0.01) between the overturning part of the freshwater transport at 26.5^{o}N and the AMOC (Fig 7c), but there are no significant relationships between the total freshwater transport and AMOC at 26.5^{o}N (R=-0.25, p=0.55, Fig 7d) or for any freshwater components at 50^{o}N (not shown). The fact that relationships between the AMOC and freshwater transports are less significant than for heat transports could be because there is, historically, less salinity data to assimilate than temperature and so uncertainties can be expected to be bigger. It is also possible that the distribution of salinity within the ocean results in a greater dominance of the horizontal component.

4 Variability

4.1 Heat and Fresh Water Content

The temperature and salinity of the upper 500m of the North Atlantic shows coherent variability (Fig 8). The subtropics (25-45^{o}N) show an increase towards warmer and more saline conditions, although there is more agreement across reanalyses in the temperature than salinity changes. This warming and salinification is consistent with anthropogenically driven trends towards a warmer and saltier subtropics, likely caused by anthropogenic changes in surface fluxes (Rhein et al., 2013). Monitoring volumetric changes above some temperature or salinity criteria can help identify thermohaline changes associated with water mass redistribution (which can change the volume of water above

this criteria) as opposed to air-sea exchange (which only directly change the near-surface temperature or salinity) (Palmer & Haines, 2009; Evans et al., 2017). However we note that assimilation could also cause volumetric changes. This volumetric analysis is shown in Fig 8 using the volume of water greater than 10^oC or 35.3 PSU; these criteria are chosen to represent the subtropical pycnocline. Some reanalyses show an increase in the volume of warm water in the subtropics, particularly since 2000, suggesting that water mass redistribution (such as advection) may also be playing a role, however this signal is not consistent across reanalyses.

In the subpolar region (45-65°N) there is an increase in temperature and salinity from the mid 90s to around 2005, and then a decrease, with the largest cooling seen in 2014. The volumetric analysis shows similar changes, suggesting a role for advection in these decadal scale changes. This is in agreement with previous studies showing the warming and cooling of the subpolar gyre through changes in advection (Robson et al., 2012; Piecuch et al., 2017; Robson et al., 2016; Hermanson et al., 2014). However we note that the large cooling seen in 2014 has been attributed to surface fluxes (Grist et al., 2016; Josey et al., 2018). There are other interannual signals such as the coherent subtropical cooling and subpolar warming in 2010. The subtropical cooling has previously been shown to have been driven by a weak AMOC and hence heat transport at 26.5^oN (Cunningham et al., 2013) with an important contribution driven by wind variations (Evans et al., 2017).

4.2 Convection and formation of deep water masses

Figure 9 shows anomalous densities in the upper (0-500m) and lower (1500-1900m) Labrador Seas waters. There are significant differences between the densities of reanalyses, but most capture the general trends. Most show a decrease in 0-500 m density in the late 90s and a strong increase after 2014. In the 1500-1900 m layer most reanalyses show a reduction in density since the mid 90s, although the timing and magnitude of weakening are varied. However, some reanalyses also appear to have unrealistic trends that do not agree with the observations; e.g. ORAS5 has a very large initial decline in deep density; GONDOLA100A has a positive density trend at depth. It should be noted, however, that there is less observational data in the LS, particularly in winter, prior to the introduction of Argo in the early 2000s. Hence there are uncertainties in the observational products: an indication of the uncertainty is given by the differences in the two observational products (EN4 and CORA).

The density of sea water is a product of the non-linear interaction between temperature, salinity and pressure, and is complicated by the fact that temperature and salinity effects are often largely compensated (Robson et al., 2016). Recently it has been shown that systematic biases in the mean state and variability of temperature and salinity in the Labrador Sea in both free-running models and reanalyses can change whether temperature or salinity has the dominant control on density changes (Menary et al., 2015, 2016; Menary & Hermanson, 2018) . Furthermore, Menary and Hermanson (2018) showed that uncertainty in this relationship has important implications for initialising and evaluating near-term climate predictions. Therefore, we evaluate whether temperature or salinity dominates the variability in the Labrador Sea densities by computing the relative correlation between density anomalies (i.e. including both changes in temperature and salinity), and the density anomalies that would result from only changes in temperature or salinity. Figure 10 shows whether temperature or salinity dominate the density variability for all the different ocean reanalyses (see caption for details). In observations the density variability of surface waters (0-200m) is mostly driven by salinity variability, however in deeper layers the density variability is mostly driven by temperature variability. Most models agree with the observations in terms of the density drivers, however there are some significant outliers. NorCPM-v1 is always temperature dominated, probably because its mean state is not constrained. GONDOLA100A, GECCO2 and ECCO V4 R3 also all have salinity dominated density anomalies at depth, which likely explains the lack of a weakening trend in their representations of densities in the 1500-1900 m layer (Fig 9b, 14b). The greater spread at depth is likely because there are less observations there to constrain the ocean properties.

For mixed layer depth (MLD) in the Labrador Sea (Fig 9c) there is initially a large spread of values with many reanalyses showing large inter-annual variability, suggesting an inability to realistically simulate the MLD. Despite the initially large variability, there is increasing consistency with time (apart from NorCPM-v1) suggesting an improvement in representation of deep convection as observational coverage increases (around the time of the introduction of Argo in the mid 2000s). Many reanalyses show a temporary deepening in mixed layer depth in 2008 and then a sustained deepening since 2010, consistent with the increase in upper ocean densities and in agreement with observations of MLD (Vage et al., 2008; Yashayaev & Loder, 2017).

4.3 AMOC Circulation

Figure 11 shows the timeseries of the AMOC at 26.5 and 50^{o}N, which are representative of the variability within the subtropical and subpolar regions respectively (not shown). As well as the timeseries of individual reanalyses, the figure also shows an ensemble mean and spread (2 x standard deviation) of the anomalies relative to each climatology. This allows an assessment of how much the variability agrees across the reanalyses.

In winter 2009/10, a substantial temporary weakening of the AMOC at 26.5^{o}N was observed, linked to a strongly negative NAO. This is suggested to have been caused by both Ekman (through the zonal wind stress) and wind-driven non-Ekman (through wind-driven upwelling of density surfaces) components (McCarthy et al., 2012; C. D. Roberts et al., 2013a). All reanalyses show a temporary weakening of the AMOC (see first column in Fig 11g) although this weakening is less than observed in most cases. The dips captured in winters 2009/10 and 2012/13 can be partially attributed to the Ekman component (blue line in Fig 11e) with many reanalyses failing to capture the non-Ekman weakening in 2009/10 (not shown). All reanalyses show a weakening of the AMOC from 2006-2013 (most of which are significant compared to the internal variability of each timeseries, see methods), in agreement with the observations, although the magnitude of weakening is again generally smaller than in the observations (Fig 11g). All reanalyses also show a brief weakening from 1999-2001 (although this is only significant in one reanalysis) and then a strengthening (mostly significant) from 2001-2006.

Prior to 1999 the reanalyses show a larger spread in the AMOC strength at 26.5^{o}N implying greater uncertainty. The consistency of the variability across the reanalyses since 1999 suggests a common driving factor, and supports the results by Jackson et al. (2016) that the observed AMOC decline may have been preceded by an increase. There is no consistent trend over the whole period (Fig 11h), although this does not preclude a longer term weakening trend. In an ensemble of forced models, Danabasoglu et al. (2016) found that the AMOC at 26.5^{o}N strengthened in the couple of decades before 1998 and then showed a significant weakening from 1998-2007 in half the models. Inspection of the timeseries (Fig. 1 in Danabasoglu et al. (2016)), however, shows that this weakening mostly occurs in the few years after 1998, with the multimodel mean showing a weakening of 2-3Sv between 1998-2004. This is similar to the weakening seen in our ensemble around

year 2000, although occurring over a longer period of time. A recent study looking at the AMOC in a different ensemble of reanalyses (Karspeck et al., 2017) found little agreement with the AMOC observed at 26.5^{o}N, contrary to results here. We note that Karspeck et al. (2017) only considered reanalyses over the period 1960-2012 when there was little data to assimilate for the majority of the period. Therefore many of the reanalyses did not assimilate more recent sources of data such as altimeter data. This study considers a more diverse set of reanalyses, only a few of which overlap with, or have predecessors in, the Karspeck et al. (2017) study.

A more in depth comparison with the RAPID observations is made in Fig 12 which shows the correlations with the observational array and standard deviations for the AMOC components. Out of those reanalyses where this comparison is possible, the best correlations with the RAPID observations are achieved with the four NEMO 0.25 reanalyses and ECCO V4 R3. It is perhaps not surprising that there is agreement amongst the NEMO reanalyses (since they use the same ocean model and observations for assimilation), however it should be noted that they still show a range of values for the changes and trends in Fig 11g,h. ECCO V4 R3 however is a very different reanalysis in that it uses a different ocean model (MITgcm) and assimilation scheme. Most reanalyses also underestimate the interannual variability. It should also be noted that the components of the upper and lower limbs of the AMOC (apart from the Ekman component which is determined by the wind fields used) compare less favorably to the observations than the total (Fig 12). Although the Ekman component contributes to the agreement of the total AMOC to the observations, there is also better agreement of the AMOC minus the Ekman transport with observation (not shown) than any of the individual components. This suggests that the resemblance to observations is through some constraint (as yet unknown) of the system on the total transport, rather than through capturing individual components, ie resolving the Florida Straits flow and getting the depth structure of the deep AMOC return flow (see also Forget (2010); C. D. Roberts et al. (2013a); Kohl (2015); Jackson et al. (2016))

At 50^{o}N the variability is consistent across most reanalyses although there are a wide range of mean strengths (Fig 11b,d,f and Fig 2). Much of this interannual variability is from the wind-driven Ekman transport (Fig 11f shows the Ekman transport calculated from GloSea5). It is to be expected that the Ekman transport would be similar across the reanalyses since it is essentially prescribed through wind fields (though mod-

ified by ECCO V4 R3 and GECCO2). Most of the reanalyses show significant weakening between 1993 and 2009 (Fig 11b,d,f,h) consistent with other studies suggesting a weakening over that period caused by density decreases in the Labrador Sea (Robson et al., 2012; Danabasoglu et al., 2016; Robson et al., 2016). This weakening is not seen in the Ekman component, but is seen in the multi-model mean minus the Ekman component (red line in Fig 11f). The magnitude of weakening is of a similar magnitude to trends in the AMOC at 45^oN from 1995-2007 in an ensemble of forced ocean models (multimodel mean -0.15 Sv/year, Danabasoglu et al. (2016)) and a previous ensemble of reanalyses (multimodel mean $\sim$-0.16 Sv/year Karspeck et al. (2017)). Most reanalyses also show a significant weakening for the longer period 1993-2016 (not shown).

Recent observations by the OSNAP array have measured the AMOC in the subpolar gyre. This is across a line stretching from Newfoundland, Canada to the southern tip of Greenland and then to Scotland and measures the AMOC in density space. Since there are only 21 months of observations currently we do a comparison of monthly values in Fig 13d. Those reanalyses for which this calculation was done show very similar variability, with a minimum in winter 2014/15 followed by an increase in spring/summer 2015, and a gradual weakening to winter 2016. Although the timing of the variability fits with the seasonal cycle of most reanalyses (Fig 13c), the magnitude of the observed changes is much larger than the seasonal cycle: in particular the minimum in winter 2014/15 is unusually low compared to the rest of the period since 1993. We hypothesize that the monthly variability since 2014 is wind-driven (though not Ekman driven, see Lozier et al. (2019)), which could explain the ability of the reanalyses to reproduce it consistently. Interannual to decadal changes (Fig 13b) are more diverse. Most of the reanalyses show some coherence in variability since 2006, with a weakening in 2008/2009, increasing abruptly around 2009/2010 (which is possibly associated with the strong negative NAO that caused the weakening at 26.5^oN (McCarthy et al., 2012; C. D. Roberts et al., 2013a)), then weakening again in 2012. However prior to 2006 there is little consistency in the signals. We note that the increase around 2010 is similar to that seen in the AMOC in depth space at 50^oN (Fig 11b,d,f), however the OSNAP section does not otherwise show the same consistent interannual variability.

Many studies have shown relationships between the AMOC strength and the density in the Labrador Sea over decadal timescales (Jackson et al., 2016; C. D. Roberts et al., 2013b). About half of the reanalyses show a weakening trend in the 0-500m LS den-

sity from 1993-2009 (although about half show little trend), and most show a weakening trend in 1500-1900m density. Observational products agree that there was a density decrease over this period at both depths. Most reanalyses also agree that there was a weakening of M50, but there is no significant relationship found across the reanalyses between the trends in either 0-500m density or 1500-1900m density, and the trends in M50 (Fig 14a,b). This suggests that either the sensitivity of the AMOC weakening to the density weakening varies across the ensemble or that there is no direct relationship within the reanalyses. This may be because aspects of the assimilation modify the relationship. It is also possible, however, that there would be a stronger relationship with a different density metric, for instance some models and reanalyses have shown a relationship with the GIN seas density or using a lagged correlation (Ba et al., 2014; Storto et al., 2016). Recent observations of overturning in the subpolar gyre have found that the majority of the overturning occurs to the east of Greenland, raising questions as to how relationships between the Labrador Sea density and AMOC strength should be interpreted (Lozier et al., 2019).

Studies of decadal variability have shown lagged relationships of the AMOC at different latitudes, with the AMOC in the SPG preceding that at 26.5^{o}N (Williams et al., 2014; Yeager & Danabasoglu, 2014). We do not have sufficient years to examine correlations between the two timeseries, however we note that Jackson et al. (2016) suggested that the weakening of the SPG AMOC since the mid 90s was related to the later observed weakening of the AMOC at 26.5^{o}N. Hence we compare the magnitudes of weakening between these two events (Fig 14d), but see no relationship across reanalyses.

4.4 Gyre Circulation

Anomalies of the SPG and STG strengths are shown in Fig 15. These are defined as the maximum of the barotropic streamfunctions over 60-30^{o}W, 50-60^{o}N (SPG) and 80-50^{o}W,25-38^{o}N (STG). For the SPG there is a weakening (positive trend in the streamfunction) up to 2009 seen in the ensemble average. All ensemble members show this positive trend which is significant in most of the members (Fig 15g). For the trend to 2016 GONDOLA100A disagrees with the rest of the ensemble in having a significant strengthening (negative trend). The weakening of the subpolar gyre from a maximum in the mid 90s has also been seen in many previous studies (Boning et al., 2006; Lohmann et al., 2009; Danabasoglu et al., 2016). An index of subpolar gyre strength based on observed

sea surface heights (Häkkinen & Rhines, 2004) also shows a weakening since the mid 90s, however modified definitions of the gyre index have shown a partial recovery since 2010 (Foukal & Lozier, 2017; Hatun & Chafik, 2018).

There is also a temporary strengthening of the SPG around 2009-2010. This is likely to be linked to the strong negative NAO that is associated with a weakening of the AMOC at 26.5^{o}N and a strengthening at 50^{o}N. The STG in GLORYS2v4 is very weak between 1998 and 2004, leading to a large ensemble spread over that period. Most ensemble members show a weakening of the STG from 1993-2016, however this is only significant in a couple of members (Fig 15g).

Although most reanalyses agree that there was a weakening of the SPG and M50, there is again no significant relationship across the ensemble (Fig 14c). A relationship between the two has been seen in other studies (Boning et al., 2006; Ba et al., 2014; Danabasoglu et al., 2016). Yeager (2015) show that this relationship is through the interaction of deep densities with the topography.

4.5 Transports

Heat transports at 26.5^{o}N are strongly dominated by the overturning component with little transport by the horizontal circulation component (Fig 16). This is in agreement with observations and other modeling studies (Johns et al., 2011; Msadek et al., 2013; Danabasoglu et al., 2016). We find strong correlations between the AMOC trends over 2005-2015 and the trends in both overturning and total heat transports ($R > 0.86$, $p < 0.01$, Fig 18a,b). The reanalyses also show strong correlations of the interannual AMOC and heat transport timeseries within each reanalysis at 26.5^{o}N (Fig 18e). Regression coefficients of annual means in those reanalyses where the comparison is significant are between 0.04-0.08 PW/Sv with the observations being within this range (0.07 PW/Sv). A comparison with forced ocean models gives similar values (Danabasoglu et al., 2016), and the regression coefficient when comparing trends (Fig 18b) is also within this range (0.05 PW/Sv). This evidence all points to a strong relationship between the AMOC at 26.5^{o}N and the heat transport at this latitude.

We also note that there is some correspondence between periods where the heat transports are high (1999, 2006-2008, 2012) with periods when there is an increase in subtropical temperature, and periods where heat transports are low (2000, 2010-2013)

with periods of subtropical cooling (Fig 8a and 16a). Surface heat fluxes can also be important in changing the temperature of the region, and reanalyses also have changes in heat from the assimilation of data. A rigorous examination of the heat budget across reanalyses would require a comparison of assimilation terms, as well as surface fluxes, and hence is difficult for a multi-model ensemble of reanalyses.

For freshwater transport, although there is a good relationship between the AMOC and the overturning transport component at 26.5^{o}N ($R = -0.92$, $p < 0.01$, Fig 18c), the horizontal transport component also plays an important role in the variability and strength of the freshwater transport, which prevents any clear relationship of the AMOC with the total transport ($R = -0.28$, $p = 0.54$, Fig 18d).

At 50^{o}N most of the variability and strength of the heat and freshwater transports depends on the horizontal part, rather than the overturning part of the transport (Fig 17). However we note that the thermohaline circulation, which represents the circulation resulting from water mass transformation, has a strong horizontal component in the subpolar region, rather than being predominantly in the overturning component (Yeager, 2015).

There is a clear weakening seen in the horizontal and total heat transport at 50^{o}N from the mid 90s (see Fig 17). Strong transports of heat and freshwater near the start of the period are consistent with the warming and salinification seen in the subpolar gyre, and weaker transports towards the end of the period are consistent with a cooling and freshening (Fig 8). We note that surface fluxes also play a role and that the recent cooling since 2014 in the subpolar gyre has been linked to surface cooling (Grist et al., 2016; Josey et al., 2018).

Although there is a significant correlation between the trends of AMOC and overturning transport of heat at 50^{o}N ($R = 0.83$, $p = 0.02$), this is not a significant contribution to the trend in total heat transport (Fig 17). Indeed there is no significant relationship between the trends in AMOC or SPG and trends in total heat or freshwater transports at 50^{o}N (not shown). In most individual reanalyses there are significant correlations between the total heat transport timeseries and both the AMOC and SPG timeseries, but this is likely because these timeseries all have trends (Fig 18e).

5 Discussion and conclusions

We have presented results from examining the mean state and variability of the North Atlantic since 1993 from an ensemble of global ocean reanalyses. The results here are relevant to those using and developing the reanalyses and those wanting to understand how and why the North Atlantic has changed recently. We focus our discussion and conclusions on the questions introduced in the introduction.

5.1 Where is there agreement or disagreement across reanalyses?

Reanalyses are able to capture many aspects of the dynamics in the North Atlantic. In particular:

- Although there is large disagreement among reanalyses in the Labrador Sea mixed layer depth initially, this improves in time. This is likely to be because of greater observational constraints later in the period (eg the introduction of Argo in the mid 2000s).
- There is consistency across the ensemble of variability in the AMOC at both 26.5 and 50^{o}N (and agreement of the former with independent observations). This is in contrast with a previous study (Karspeck et al., 2017) that found little agreement of reanalyses over an earlier, more observation-sparse period. There is also agreement of monthly variability with new observations of overturning in the subpolar North Atlantic.
- At 26.5^{o}N the reanalyses mostly agree with the independent observational estimates of mean AMOC strength. However they underestimate the ocean heat transport (OHT) per Sverdrup of volume transport, despite having a strong correlation between AMOC and OHT. This discrepancy has previously been seen in ocean models (Danabasoglu et al., 2014).
- The reanalyses using NEMO at 0.25 and 1/12^o have more intense Gulf Streams and stronger transports of heat and freshwater from 30-50^{o}N. These differences may be because they have higher horizontal resolutions (eddy-permitting and eddy-resolving).
- NorCPM-v1 is an outlier in the mean comparisons because it uses anomaly assimilation. GECCO2 is also an outlier in several comparisons, particularly of variability. This may be because it was run over several short (5 year) windows. ORAS5

has a large change in Labrador Sea density and AMOC strength from 1996-2000 which is associated with extra buoyancy loss caused by SST nudging and sparse in-situ observations in the early period (Tietsche, personal comm).

5.2 Can we learn what makes reanalyses good at specific processes?

- A greater availability of observations can improve the representation of processes. In particular mixed layer depths within the Labrador Sea improve over the latter half of the period studied. There is also a greater agreement among the reanalyses (and with observations from 2004) of the variability of AMOC strength at 26.5N than in a previous study looking at an earlier, more observation-sparse period.
- Some reanalyses have density variability in the deep Labrador Sea that is driven by salinity, rather than temperature, variability. This may affect their ability to capture the observed decline and may have an impact on dynamics. This suggests that more deep observations, such as deep Argo, are needed.
- Eddy-permitting and resolving resolution, such as used in the NEMO-based reanalyses, can strengthen western boundary currents and transports at mid-latitudes.
- ECCO V4 R3 uses a 4DVar scheme where adjustments are made to parameters such as surface forcing and ocean mixing rather than directly modifying temperature and salinity through increments. It shows similar variability to other (non 4DVar) reanalyses, and to some independent observations. This improves our confidence that both 4DVar and non-4DVar schemes can produce reasonable results. However ECCO V4 R3 does have the wrong density drivers and trends in the deep Labrador Sea water, possibly because the assimilation scheme does not directly affect deep properties and instead changes much be subducted or vertically mixed from the surface, or changes can be made by modifications of the mixing itself (for instance by changes in winds). We do note, though, that 4DVar has advantages in that it avoids direct adjustments of water masses, and is therefore more dynamically consistent.

5.3 Can these reanalyses improve our understanding of the dynamics in the North Atlantic ocean?

- Results support the subpolar picture of a decrease in Labrador Sea density, and a weakening SPG and AMOC at 50^{o}N over the period (attributed by other studies to decadal-multidecadal variability). Heat and freshwater transports also show a decline. The strong (weak) transports in 1993-2005 (2005-2016) are consistent with an increase (decrease) in temperature and salinity.
- Results support the subtropical picture of strong interannual variability, with a gradual warming and salinification consistent with anthropogenic climate change. A strong relationship between the AMOC and the heat transport at 26.5 ^{o}N is found, which in turn can impact the subtropical heat content.
- Reanalyses with denser mean upper Labrador Sea densities have a stronger mean AMOC at 50^{o}N. No relationships are found between the trends across the reanalyses. There is also no relationship found between the AMOC at 26.5 and 50^{o}N, either in mean strength or variability.
- Although there is a strong relationship between the AMOC and heat transport at 26.5^{o}N, there is no clear relationship across the reanalyses between the heat transport at 50^{o}N and the SPG or AMOC transports (either for the mean or variability).
- Reanalyses mostly agree that the AMOC at 26.5^{o}N showed a weakening from 1999-2001, followed by a strengthening from 2001-2006 and then a weakening from 2006-2013. This suggests that the observed weakening (since 2004) is part of interannual-decadal variability.
- Reanalyses mostly agree that the AMOC at 50^{o}N has interannual variability from the Ekman component superimposed on a more gradual weakening from the mid 90s.
- Reanalyses also compare well with the OSNAP section, suggesting that they may be useful tools to further understand the variability and its cause

Although many relationships found in modeling studies are not found to hold across these reanalyses, it does not mean that those relationships do not hold in reality. For example, we see trends from the mid 90s in many variables in the subpolar gyre region. These variables could be physically related and show correlations of timeseries, however

the strengths and timing of these relationships could differ across reanalyses. Hence relationships between trends are not found. It is also possible that stronger relationships would be found with different metrics, time periods or lags. In reanalyses it is also possible that relationships can be obscured or changed by spatial or temporal variations in the quality of the observational constraints. Hence to properly explore mechanisms using a reanalysis, a good understanding is required of whether relevant processes are physically consistent, or whether there are spurious impacts from the assimilation (Storto et al., 2019).

Nevertheless, reanalyses are promising tools to examine recent climate variability alongside free running ocean models (which can experience biases) and observations (which are temporally and spatially sparse). Reanalyses cannot be a replacement for observations: in particular a good observational coverage is necessary for constraining reanalyses. Independent observations, such as the AMOC transports calculated by the RAPID and OSNAP sections, are also independent checks. We note that although reanalyses are able to realistically simulate many aspects of the AMOC at 26.5^oN, they cannot simulate important details, such as the different AMOC components. Hence it is important to continue these observational campaigns, along with developing ocean reanalyses, in order to understand and monitor the ocean.

Table 1: Acronyms used

Acronym	Full name	Notes
3DVar	Three dimensional variational analysis	technique
4DVar	Four dimensional variational analysis	technique
AER	Atmospheric and environmental research	institute/group
AMOC	Atlantic Meridional Overturning Circulation	physical quantity
BBL	Bottom boundary layer	technique
BCCR	Bjerknes centre for climate research	institute/group
BSF	Barotropic streamfunction	physical quantity
CICE	Sea ice model	model
CLIVAR	Climate Variability and Predictability	institute/group
CMCC	Centro Euro-Mediterraneo sui Cambiamenti Climatici	institute/group
CORA	Coriolis ocean dataset for reanalysis	ocean observational product
ECMWF	European Center for Medium-range Weather Forecasting	institute/group
EN4	EN4	ocean observational product
EnKF	Ensemble Kalman filter	technique
ERA	ECMWF reanalysis	atmospheric reanalysis product
FGAT	First guess at appropriate time	technique
GCM	Coupled general circulation model	model
GFDL	Geophysical Fluid Dynamics Laboratory	institute/group
GODAE	Global Ocean Data Assimilation Experiment	institute/group
GSOP	Global synthesis and observations panel	institute/group
JMA	Japan meteorological agency	institute/group
JPL	Jet propulsion laboratory	institute/group
JRA	Japan reanalysis	atmospheric reanalysis product
KF	Kalman filter	technique
LIM	Louvain-la-Neuve Sea Ice Model	model
LS	Labrador Sea	physical quantity
M26	AMOC strength at 26.5N	physical quantity
M50	AMOC strength at 50N	physical quantity
MICOM	Miami Isopycnal Coordinate Ocean Model	model
MIT	Massachusetts Institute of Technology	institute/group

MITgcm	MIT general circulation model	model
MLD	mixed layer depth	physical quantity
MOCHA	Meridional overturning circulation and heat-flux array	ocean observational product
MOM	Modular Ocean Model	model
MRI	Meteorological Research Institute	institute/group
MRI.COM	Meteorological Research Institute Community Ocean Model	model
NAO	North Atlantic Oscillation	physical quantity
NCEP	National center for environmental prediction	atmospheric reanalysis product
NEMO	Nucleus for European Modelling of the Ocean	model
NOAA	National Oceanic and Atmospheric Administration	institute/group
OBP	Ocean bottom pressure	physical quantity
OFWT	Ocean fresh water transport	physical quantity
OHC	Ocean heat content	physical quantity
OHT	Ocean heat transport	physical quantity
OI	Optimal interpolation	technique
ORA	Ocean Reanalysis	institute/group
OSNAP	Overturning in the subpolar north atlantic project	ocean observational product
RAPID	Observational array for measuring AMOC at 26.5N	ocean observational product
S	salinity	physical quantity
SIC	Sea ice concentration	physical quantity
SIS	GFDL Sea Ice Simulator	model
SIT	Sea ice thickness	physical quantity
SPG	Subpolar gyre	physical quantity
SSH	Sea surface height	physical quantity
SSS	Sea surface salinity	physical quantity
SST	Sea surface temperature	physical quantity
STG	subtropical gyre	physical quantity
T	temperature	physical quantity

Name	C-GLORSv7	ECDA3	GECCO2	GLORYS2v4	GloSea5	ECCO V4 R3	ORAS5	NorCPM-v1	UR025.4	GONDOLA100A	GLORYS12v1
Institution	CMCC	GFDL/NOAA	Hamburg University	Mercator Océan	UK Met Office	MIT/JPL/AER	ECMWF	BCCR	University of Reading	MRI/JMA	Mercator Océan
Nominal horizontal resolution	0.25°	1x1/3°	1x1/3-1°	0.25°	0.25°	1x1/3-1°	0.25°	1°	0.25°	1x 1/3-0.5°	1/12°
Vertical resolution	75 z-levels	50 z-levels	50 z-levels	75 z-levels	75 z-levels	50 z-levels	75 z-levels	53 isopycnal layers	75 z-levels	60 z-levels +BBL	50 z-levels
Top-level thickness	∼1 m	10 m	10 m	∼1 m	∼1 m	10m	∼1 m	variable	∼1 m	∼1m	∼1 m
Includes GM	N	Y	Y	N	N	Y	N	Y	N	Y	N
Ocean–ice model	NEMO3.6/LIM2	MOM4/SIS	MITgcm	NEMO3.1/LIM2	NEMO3.4/ CICE4.1	MITgcm	NEMO3.4/LIM2	MICOM/CICE	NEMO3.2/LIM2	MRI.COMv4.2	NEMO3.1/LIM2
Time period	1989–2016	1970–2017	1948–2017	1992–2016	1989–2017	1992–2015	1979–2017	1985–2010, 30 member ensemble	1989–2010	19582015	1992–2016
Initialization	C-GLORSv5	cold start	optimized	spinup	spinup	optimized	spinup	EnKF anomaly	cold start	Jan 2000 reanalysis	spinup
Source of atmospheric forcing data	ERA-Interim	NCEP RA1	NCEP RA1	ERA-Interim	ERA-Interim	ERA-Interim	ERA-Interim, NWP after 2015	Coupled	ERA-Interim	JRA55-do v1.3	ERA-Interim
DA-Method	3DVAR	EnKF	4DVAR adjoint	reduced order KF + 3DVAR	3DVAR	4DVAR adjoint	3DVAR FGAT	EnKF anomaly	OI	3DVar + robust diagnostic	reduced order KF + 3DVAR large scale bias correction to in-situ T, S
Data Assimilated	T, S, SSH, SST, SIC, SIT	T, S, SST	T, S, SSH, SST, SSS	T, S, SSH, SST	T, S, SSH, SST, SIC	T, S, SSH, SST, SSS, SIC, OBP	T, S, SSH, SST, SIC	Anomalies of T, S, SST	T, S, SSH, SST, SIC	T, S, SSH, SST, SIC	T, S, SSH, SST
Relaxation	large-scale T,S climatology	None	None	None	SSS (Haney flux). Weak relaxation to T,S climatology	None	SSS. Weak relaxation to T,S climatology	None	None	T,S climatology	None
Reference	Storto and Masina (2016); Storto et al. (2016)	S. Zhang, Harrison, Rosati, and Wittenberg (2007); Chang, Zhang, Rosati, Delworth, and Stern (2013)	Kohl (2015)	Ferry et al. (2012)	Jackson et al. (2016); MacLachlan et al. (2015); Blockley et al. (2014)	Forget et al. (2015); Fukumori et al. (2017)	Zuo, A, Tietsche, Mogensen, and Mayer (2019)	Counillon et al. (2016); Wang et al. (2017)	Valdivieso, Haines, Zuo, and Lea (2014)	Toyoda et al. (2016)	Lellouche et al. (2018)

Table 2. Description of reanalyses. 1) Notation in columns 3,6,10 of row 2 implies a zonal resolution of 1° and a meridional resolution varying from 0.5 or 1° down to 1/3° near the equator.

Acknowledgments

This work was initiated through the EU COST-EOS-1402 project which supported the development of this paper by funding project meetings, both in person and virtual. We would like to thank Aida Azcarate for organizing the funding for the meetings and would like to thank Martha Buckley, Gokhan Danabasoglu and Simon Josey for useful discussions. Jackson and Zuo were funded, and Storto partially funded, by the Copernicus Marine Environment Monitoring Service (CMEMS: 23-GLO-RAN). Haines and Robson acknowledge funding under the NERC RAPID projects RAMOC and DYNAMOC respectively, and Robson also acknowledges funding from the ACSIS project. Mignac was supported for PhD scholarship by the CAPES Foundation, Ministry of Education of Brazil (Proc. BEX 1386/15-8). Forget acknowledges support from the Simons Foundation (549931) and the NASA IDS program (6937342). Work by Piecuch was carried out under the ECCO project, funded by the NASA Physical Oceanography, Cryospheric Science, and Modeling, Analysis and Prediction programs. Wilson was funded by the NERC UK-OSNAP project (NE/K010875.1) as part of the international OSNAP programme. NorCPM-v1 reanalysis was co-funded by the Center for Climate Dynamics at the Bjerknes Center, the Norwegian Research Council under the EPOCASA (229774/E10) and SFE (270733) research projects, the NordForsk under the Nordic Centre of Excellence (ARCPATH, 76654), and the Trond Mohn Foundation under the project number BFS2018TMT01. NorCPM-v1 reanalysis received a grant for computer time from the Norwegian Program for supercomputer (NOTUR2, project number NN9039K) and a storage grant (NORSTORE, NS9039K).

Data for the figures is available to download with the DOI 10.5281/zenodo.2598509. Data from some reanalysis products are available to download from http://marine.copernicus.eu/services-portfolio/access-to-products/ under product names GLOBAL_REANALYSIS_PHY_001_025 (GLORYS2v4), GLOBAL_REANALYSIS_PHY_001_026 (C-GLORSv7, GLORYS2v4, GloSea5 and ORAS5) and GLOBAL_REANALYSIS_PHY_001_030 (GLORYS12V1).

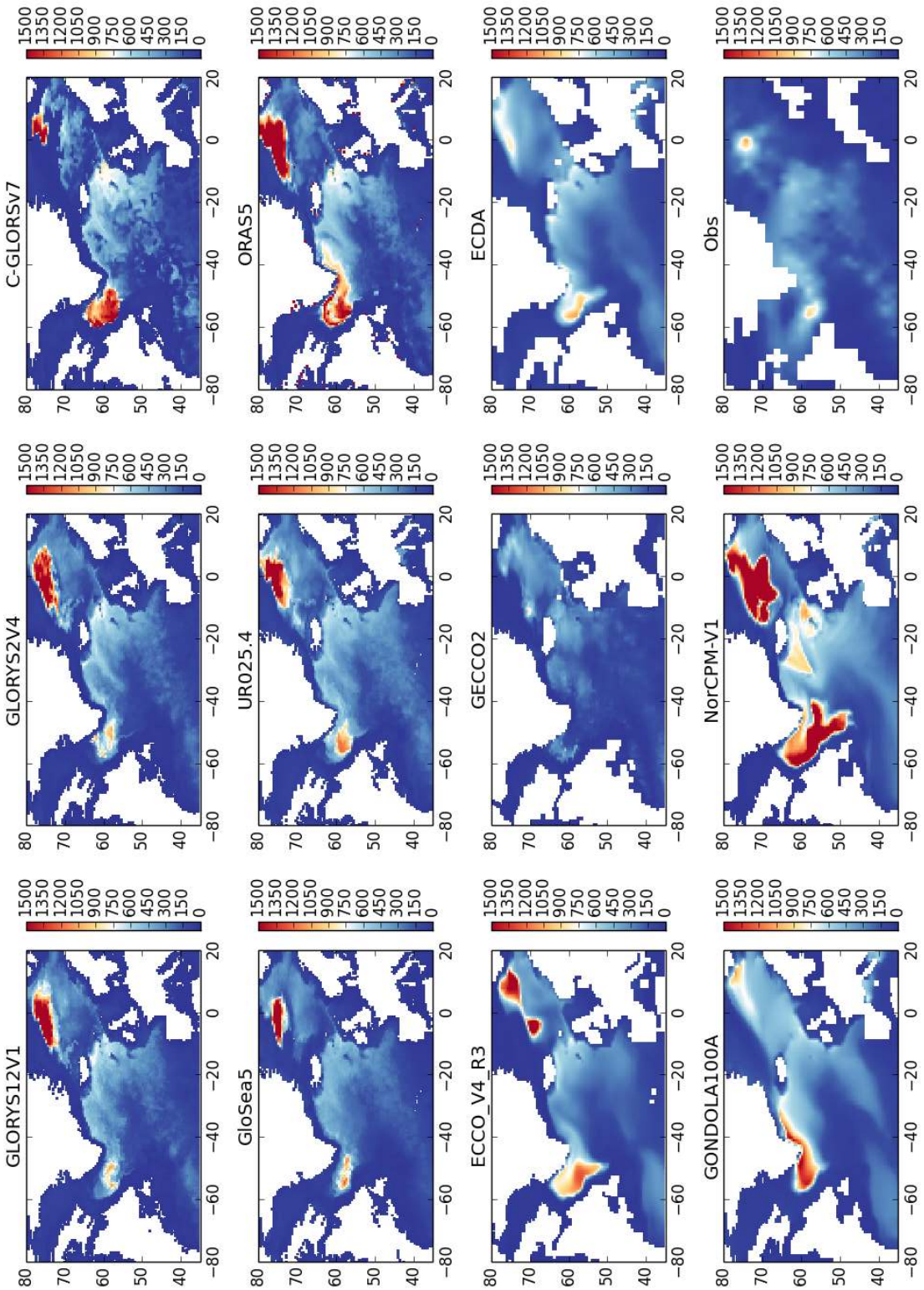

772 **Figure 1.** March mean (2004-2010) mixed layer depth (m) defined as the depth at which the
773 density differences from the surface is 0.03 kg/m^3 (calculated from monthly mean density fields).
774 The observational data set is the March mixed layer depth from de Boyer-Montegut et al. (2004).

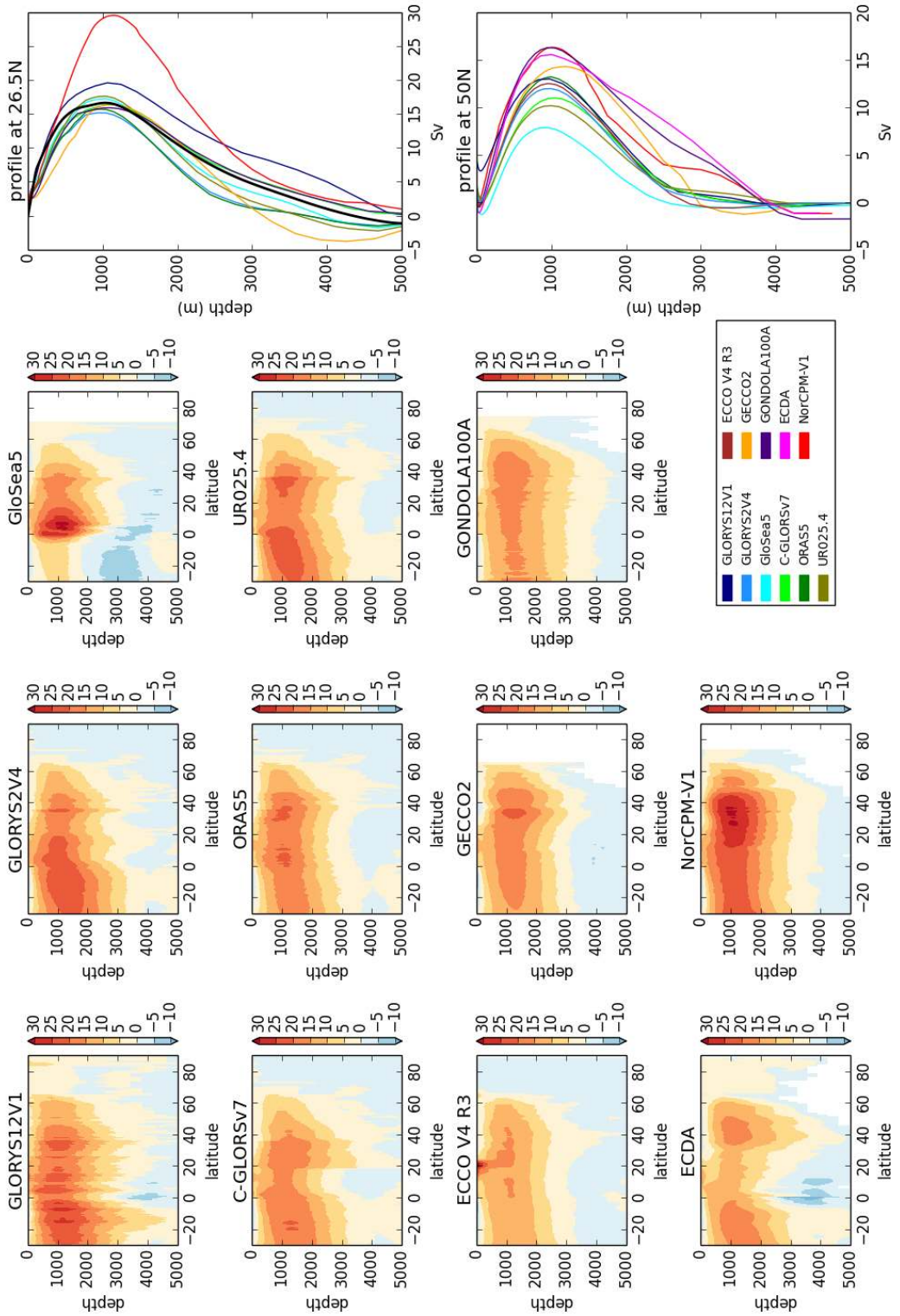

Figure 2. AMOC streamfunctions (from velocities) and profiles at 26.5^{o}N (calculated using the RAPID methodology) and 50^{o}N (from velocities). Units are Sverdrups ($Sv = 10^6 m^3/s$). Profiles use the time period 2004-2015 to agree with the observations, though the streamfunctions use the standard climatology period (1993-2010). Note that NorCPM-v1 is an outlier because it uses anomaly assimilation and hence the mean state is not constrained.

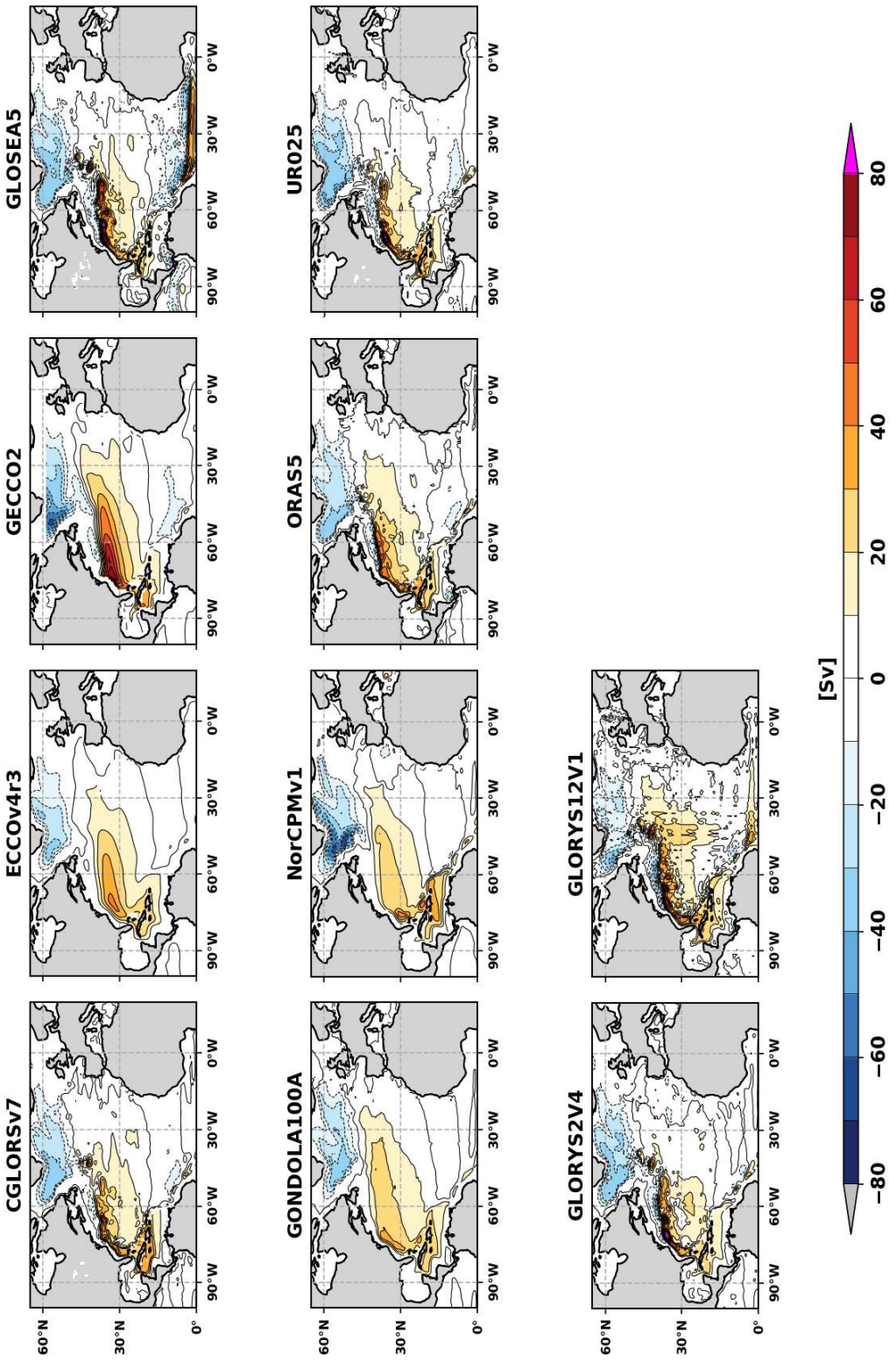

780 **Figure 3.** Barotropic streamfunctions (Sv) referenced to zero at the eastern boundary. Note
781 that NorCPM-v1 uses anomaly assimilation and hence the mean state is not constrained.

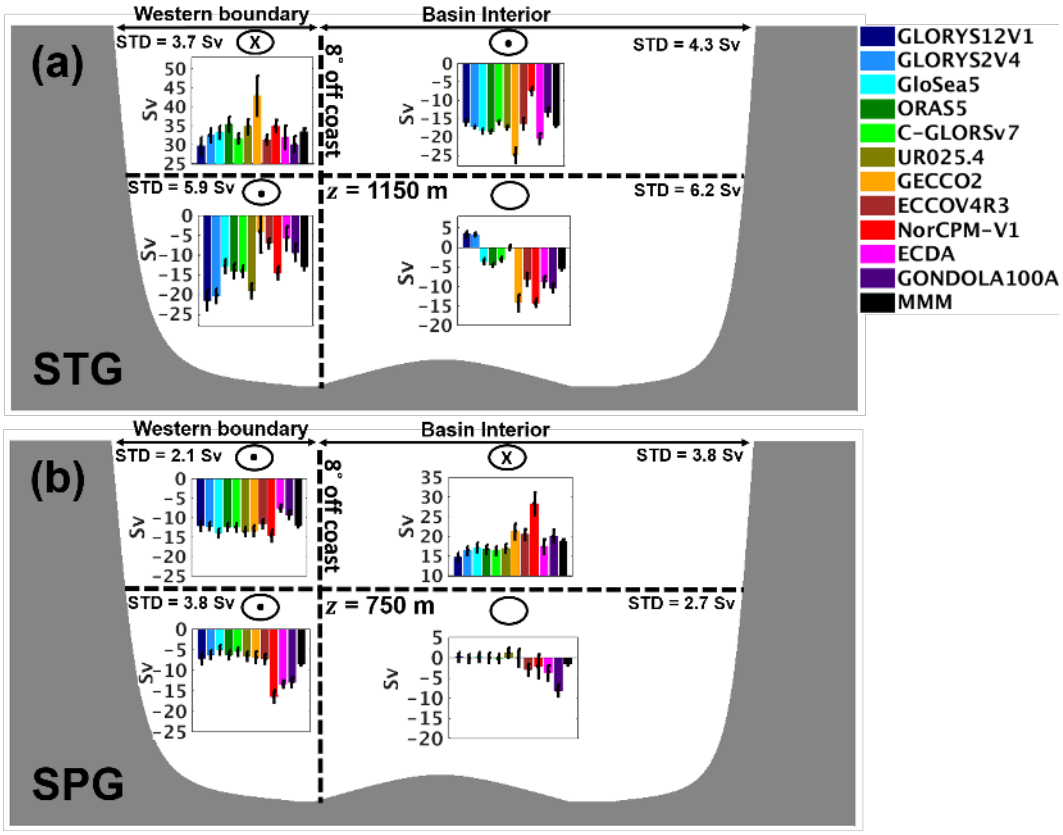

Figure 4. 4-box model of the volume transports divided into upper, lower, deep western boundary and interior flows for (a) the subtropical gyre (26^{o}N-40^{o}N), and (b) the subpolar gyre (50^{o}N-65^{o}N). Units are Sv. 8^o off the coast is chosen to separate the western boundary and interior, and the ensemble mean AMOC depth is used to separate the upper and lower limbs of the circulation for each region. The black error bars represent the uncertainty due to the varying AMOC depth between the models by using the standard deviation of the ensemble AMOC depth. The circles with dots correspond to flows going out of the page whereas the crosses represent flows going into the page. The circles without symbols mean that there is no consensus between the products about the direction of the flow. Note that NorCPM-v1 is an outlier because it uses anomaly assimilation and hence the mean state is not constrained.

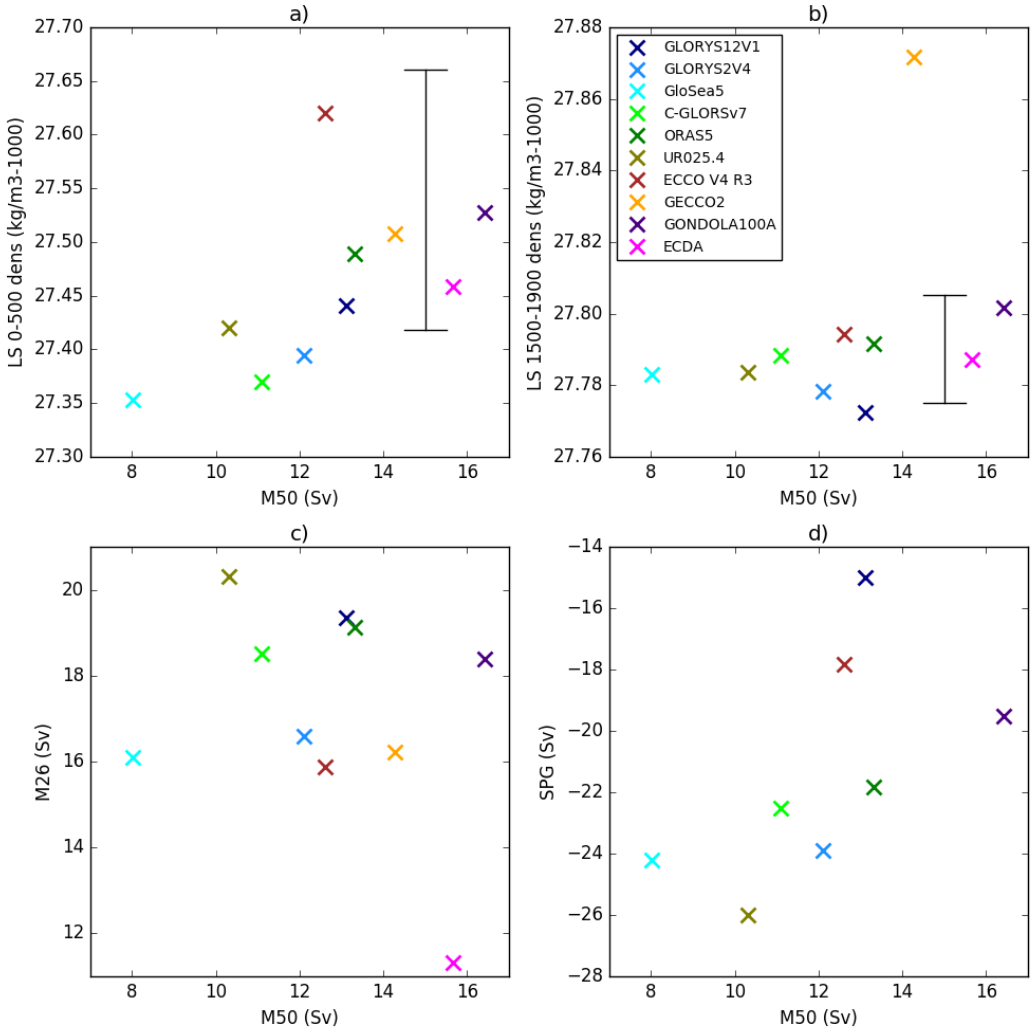

Figure 5. Comparison of the mean strengths of different variables across reanalyses (see labels). This includes the AMOC strength at 26.5^{o}N and 50^{o}N (M26,M50), the density in the Labrador Sea over 0-500m and 1500-1900m (over the region 75-40^{o}W and 50-65^{o}N), and the SPG strength. The black bars in the upper plots show the Labrador Sea densities from the EN4 and CORA observational estimates (with an arbitrary x value of M50=15Sv), with the difference indicating observational uncertainty. Note that NorCPM-v1 is not included in this analysis because it uses anomaly assimilation and hence the mean state is not constrained.

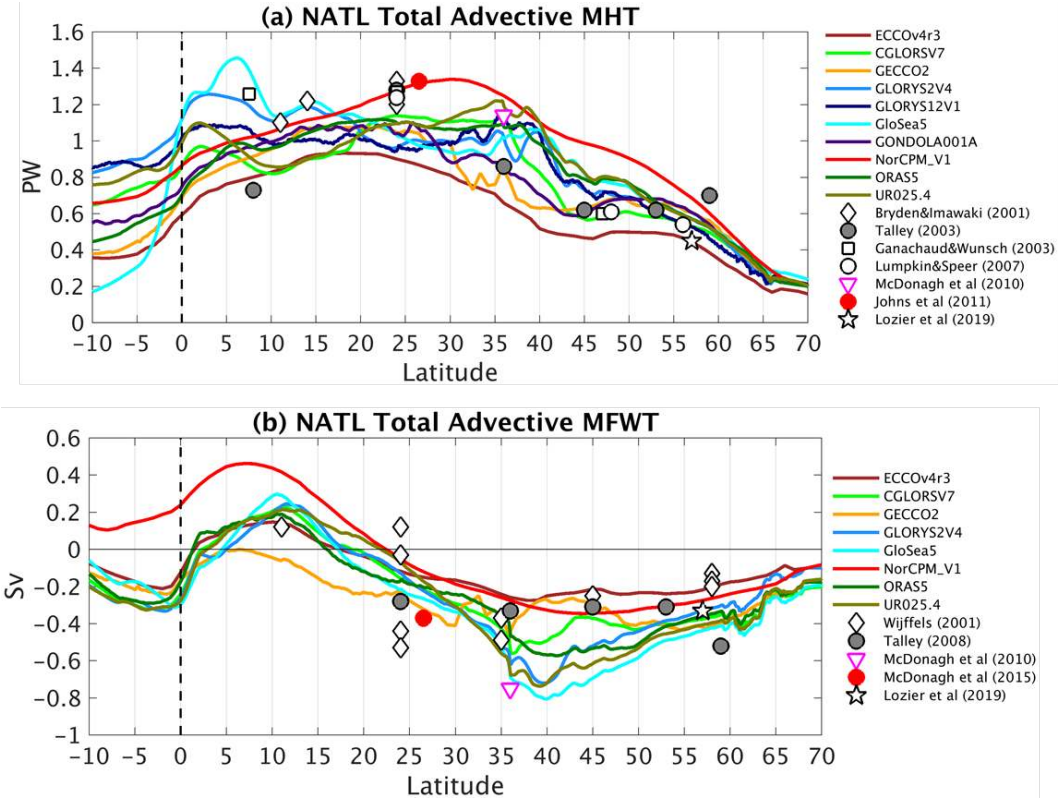

Figure 6. Mean meridional heat (top, in PW) and freshwater (bottom, in Sv) transports as a function of latitude. Also shown are observational measurements as symbols. Note that NorCPM-v1 is an outlier because it uses anomaly assimilation and hence the mean state is not constrained.

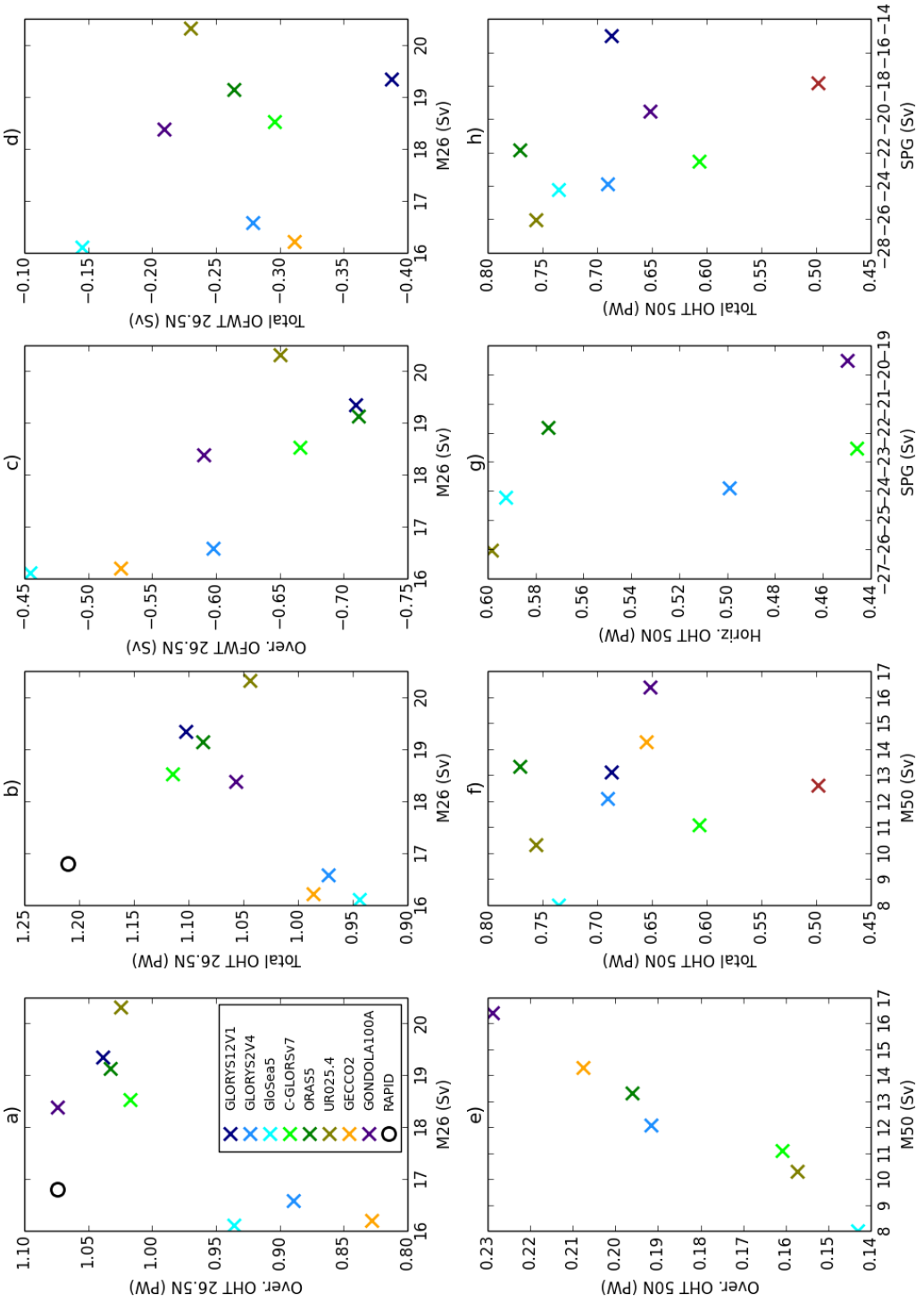

Figure 7. Comparison of the mean strengths of different variables across reanalyses (see labels). This includes the AMOC strength at 26.5°N and 50°N (M26,M50), the SPG strength and ocean heat and freshwater transports (OHT, OFWT). For the transports we also show the total transport and the overturning and horizontal components. Note that NorCPM-v1 is not included in this analysis because it uses anomaly assimilation and hence the mean state is not constrained.

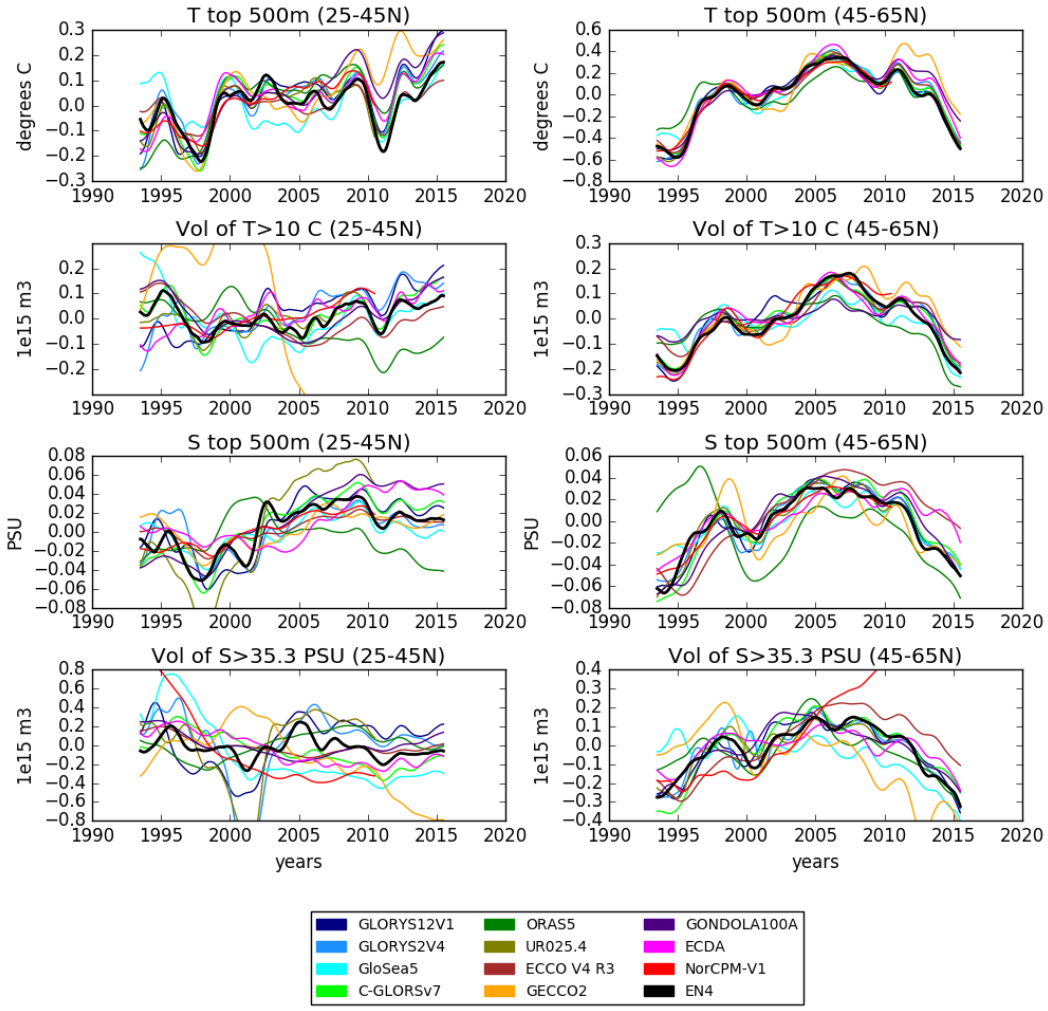

Figure 8. Anomalies of temperature (top row) in ^{o}C and salinity (third row) in PSU over the top 500m. Also shown is the volume of water (in m^3) where T>10^{o}C (second row) or S>35.3psu (bottom row). Left panels are for regions 25-45^{o}N in the Atlantic and right panels for regions 45-65^{o}N. All timeseries are anomalies with a 12 month running mean applied.

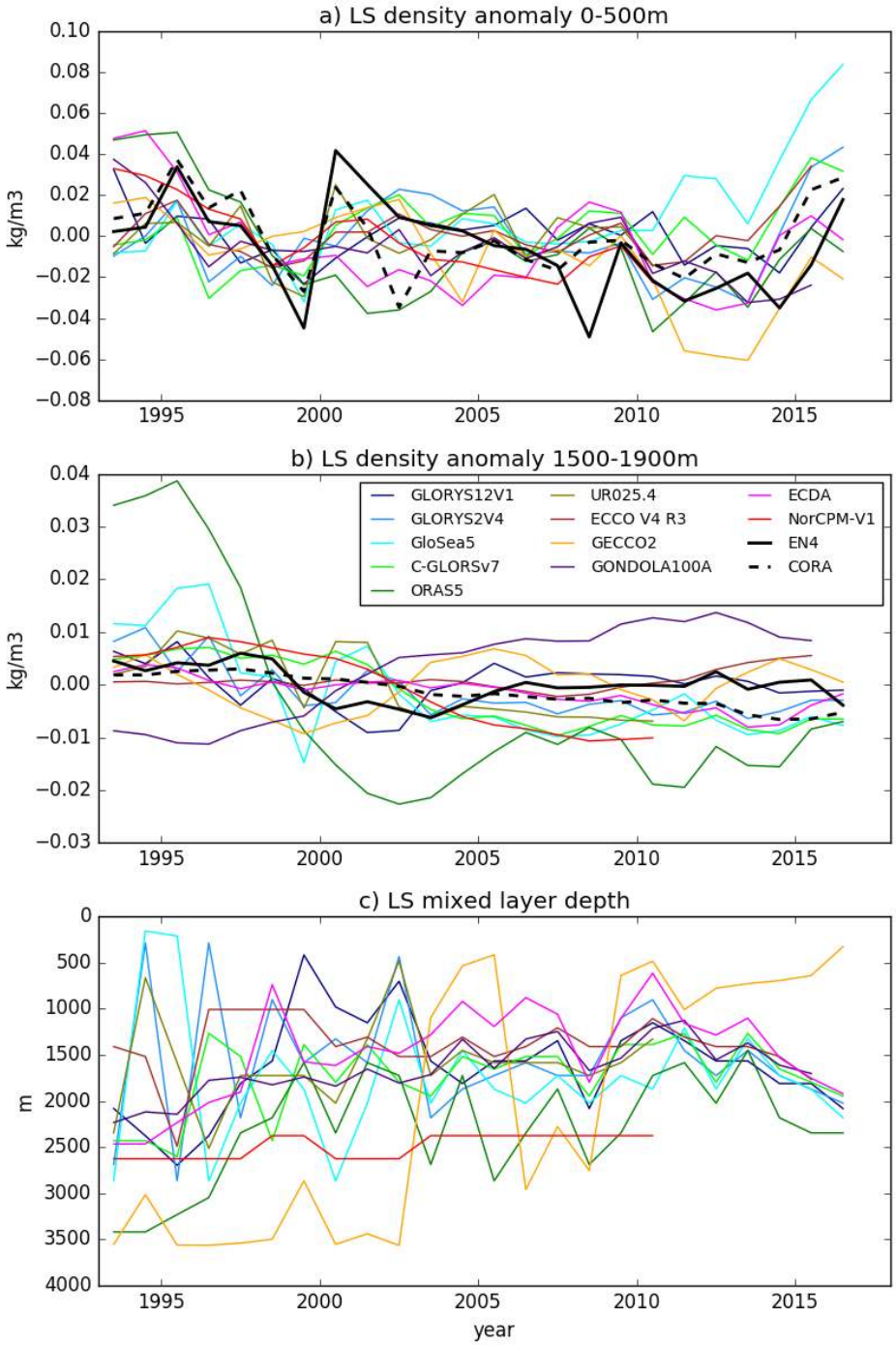

812 **Figure 9.** Time series of Labrador Sea density anomalies averaged over a) 0-500m or b)
813 1500-1900m and the region 75-40^{o}W and 50-65^{o}N. c) The maximum mixed layer depth over the
814 Labrador Sea (measured as the maximum over the region and over the year of mixed layer depths
815 defined as the depth at which the monthly mean density differs by 0.03 kg/m^3 from that at the
816 surface

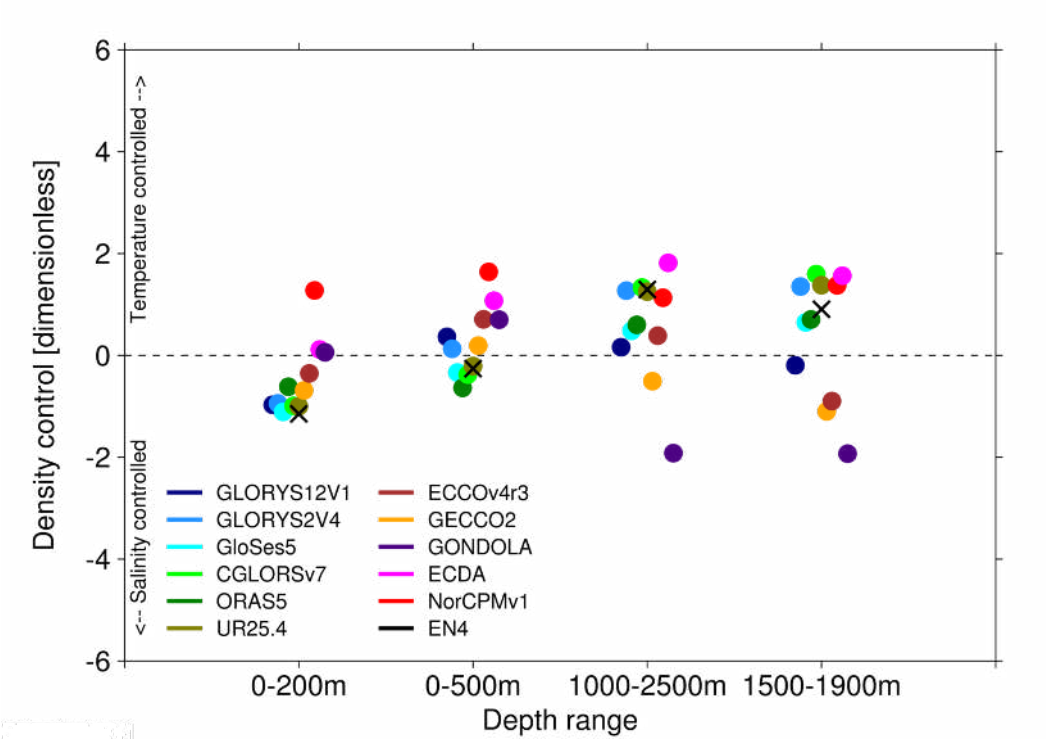

Figure 10. The relative strength of temperature or salinity in controlling density anomalies in the western subpolar North Atlantic. Positive values show density anomalies are dominated by temperature, whereas negative shows density anomalies are dominated by salinity. The density control metric is the difference between rT and rS, where rT (rS) is the correlation coefficient between the density resulting from changes in temperature (salinity) only (ie with the other variable constant), and the full density timeseries (Menary et al., 2016). Density drivers have been calculated for four different depth ranges (x-axis). The black cross shows the values from the EN4 observational analysis.

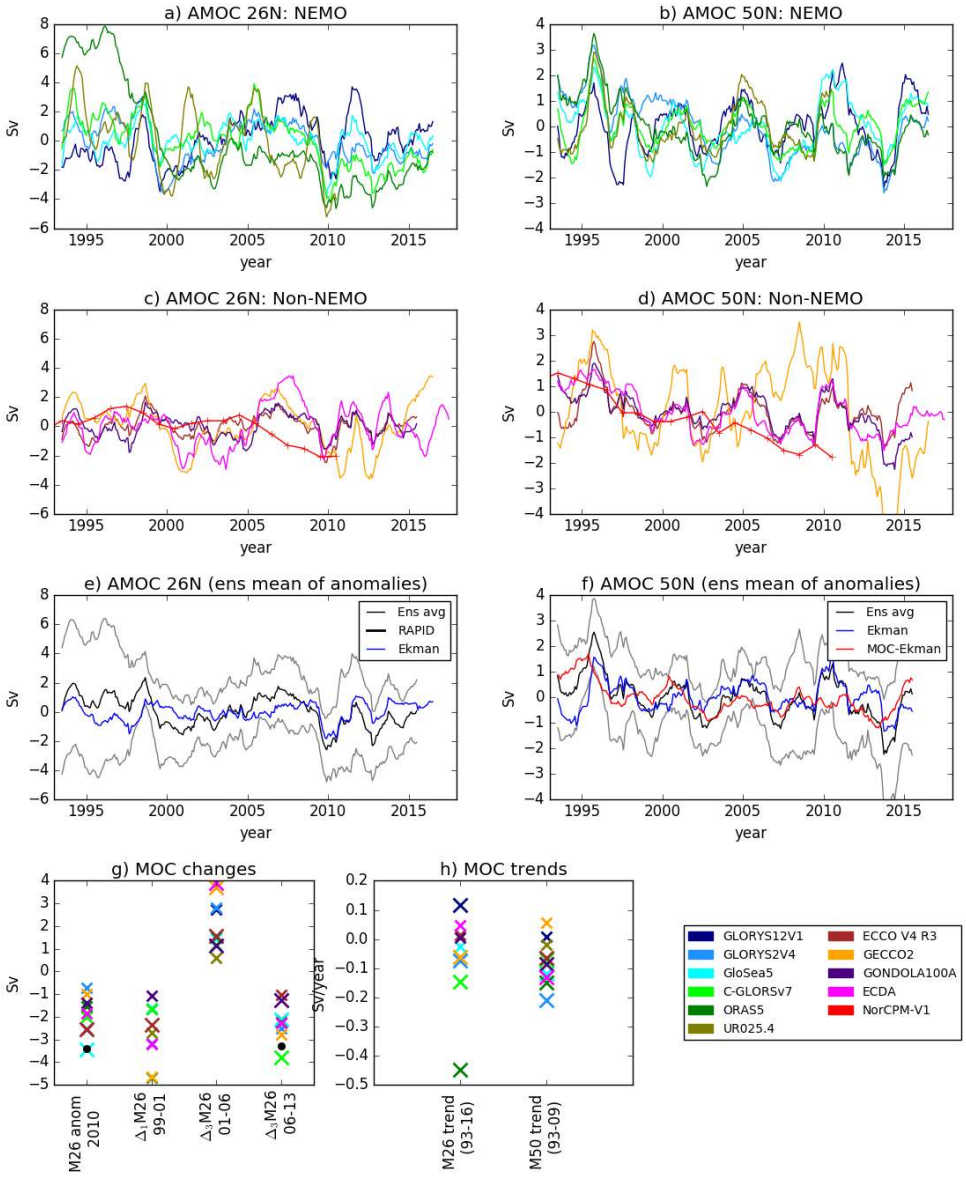

Figure 11. Timeseries of anomalous AMOC strength (with 12 month running mean). a,c) Individual models at 26.5^{o}N (thick black line is timeseries from RAPID) and b,d) at 50N. Reanalyses are split between NEMO and non-NEMO for clarity. e) ensemble mean (black) and 2 x standard deviation (grey) of AMOC anomalies at 26.5^{o}N, with the RAPID anomaly timeseries (thick black). Also shown is the Ekman transport calculated from ERA Interim winds as in C. D. Roberts et al. (2013a) (blue) f) As e but without observational timeseries and with the ensemble mean minus Ekman (red). (g,h) Comparisons of AMOC changes across the ensemble. Each cross is a model, with large crosses assessed as significant changes compared to each model timeseries. Black crosses are the changes for the ensemble mean and black circles are from the observations. g) M26 anomaly in 2009.5-2010.5 (compared to 2011-2015 time mean); M26 in 1998.5-1999.5 minus 2000.5-2001.5; M26 in 2005-2007 minus 2000-2002; M26 in 2012-2014 minus 2005-2007. f) trend in M26 (1993-2016); trend in M50 (1993-2009)

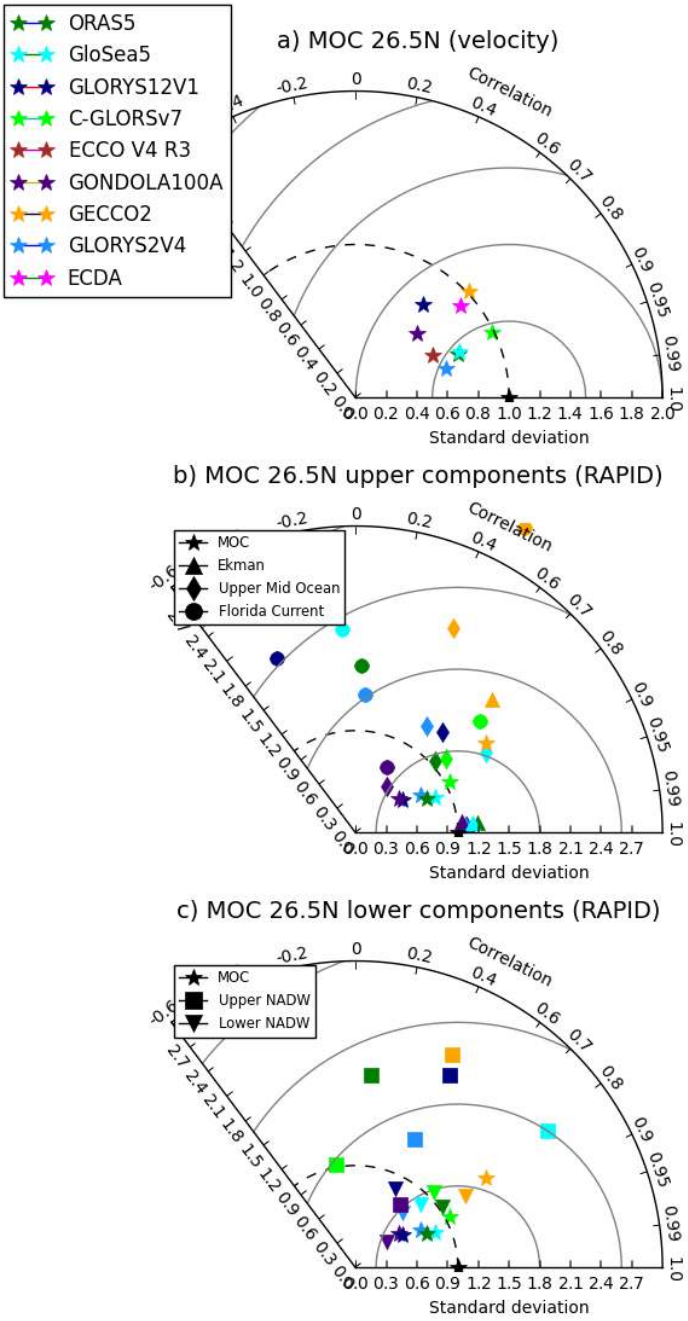

Figure 12. Taylor diagrams comparing timeseries of observations of AMOC components from RAPID, with components calculated from the reanalyses using the RAPID methodology (C. D. Roberts et al., 2013a). Shown are (a) the AMOC calculated with velocities, (b) the AMOC and upper ocean components as calculated using the RAPID methodology, (c) the AMOC and lower ocean components as calculated using the RAPID methodology. Colors show different reanalyses, symbols show different components. All standard deviations are normalized by the observational standard deviations and all statistics are calculated on annual means. Note that not all the models have calculated the RAPID decomposition and that models with insufficient years (UR025.4 and NorCPM-v1) are excluded.

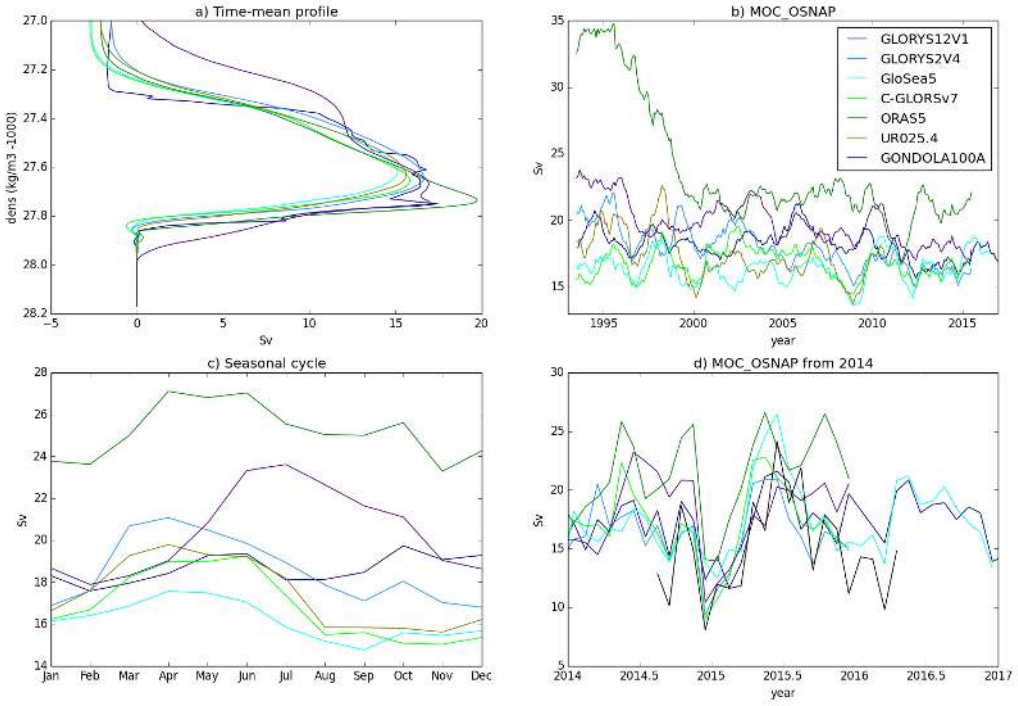

Figure 13. Overturning in density space along the OSNAP line using potential density referenced to the surface a) The time mean streamfunction in density space. b) The overturning strength (maximum in density space) with a 12 month running mean. c) Seasonal cycle of the overturning strength. d) Monthly values of last few years of overturning strength since 2014. The black line is the observational estimate from OSNAP (Lozier et al., 2019).

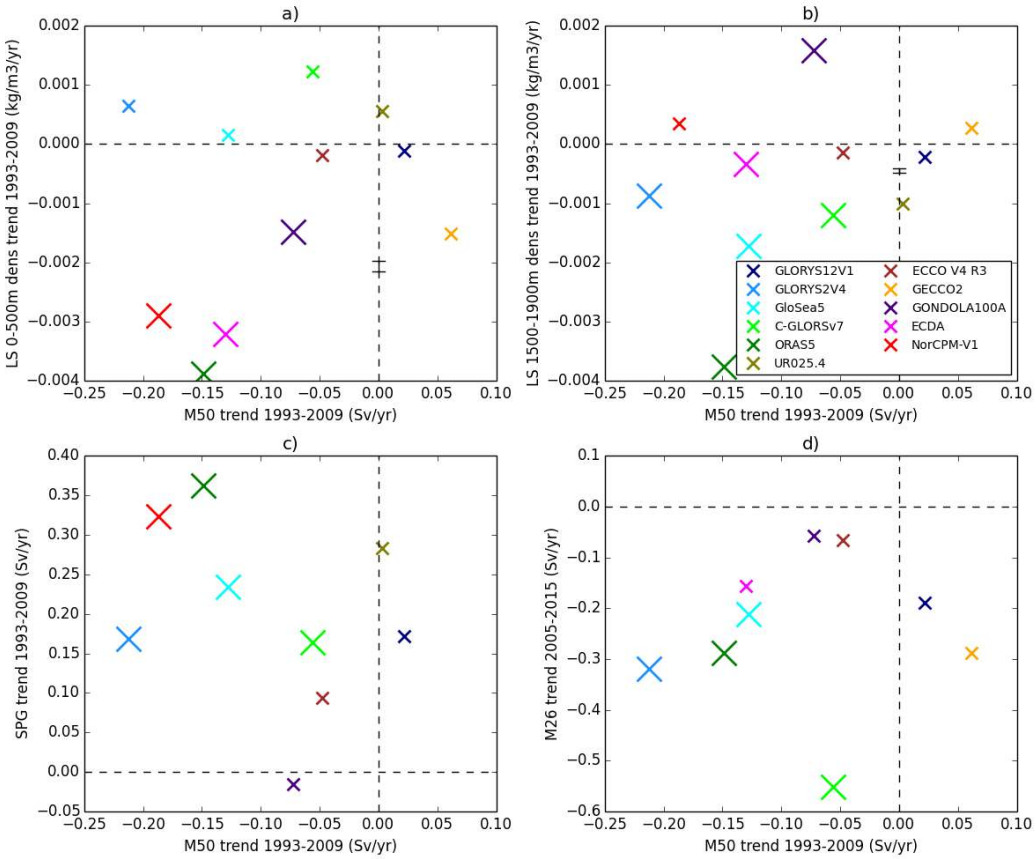

Figure 14. Comparisons of trends in the Labrador Sea density (0-500m and 1500-1900m), the SPG and the AMOC 50^{o}N (M50) over the period 1993-2009, and the trend in the AMOC at 26.5^{o}N (M26) from 2005-2015. All trends are from 1993-2009 apart from M26 which is from 2005-2015. Reanalyses where the trend in both variables is significant (using p=0.1) have large crosses. In panels a and b we also include values of density trends from EN4 and CORA observational analyses as a black bar. The bar is arbitrarily centered on x=0. Dashed lines indicate the lines of zero trend.

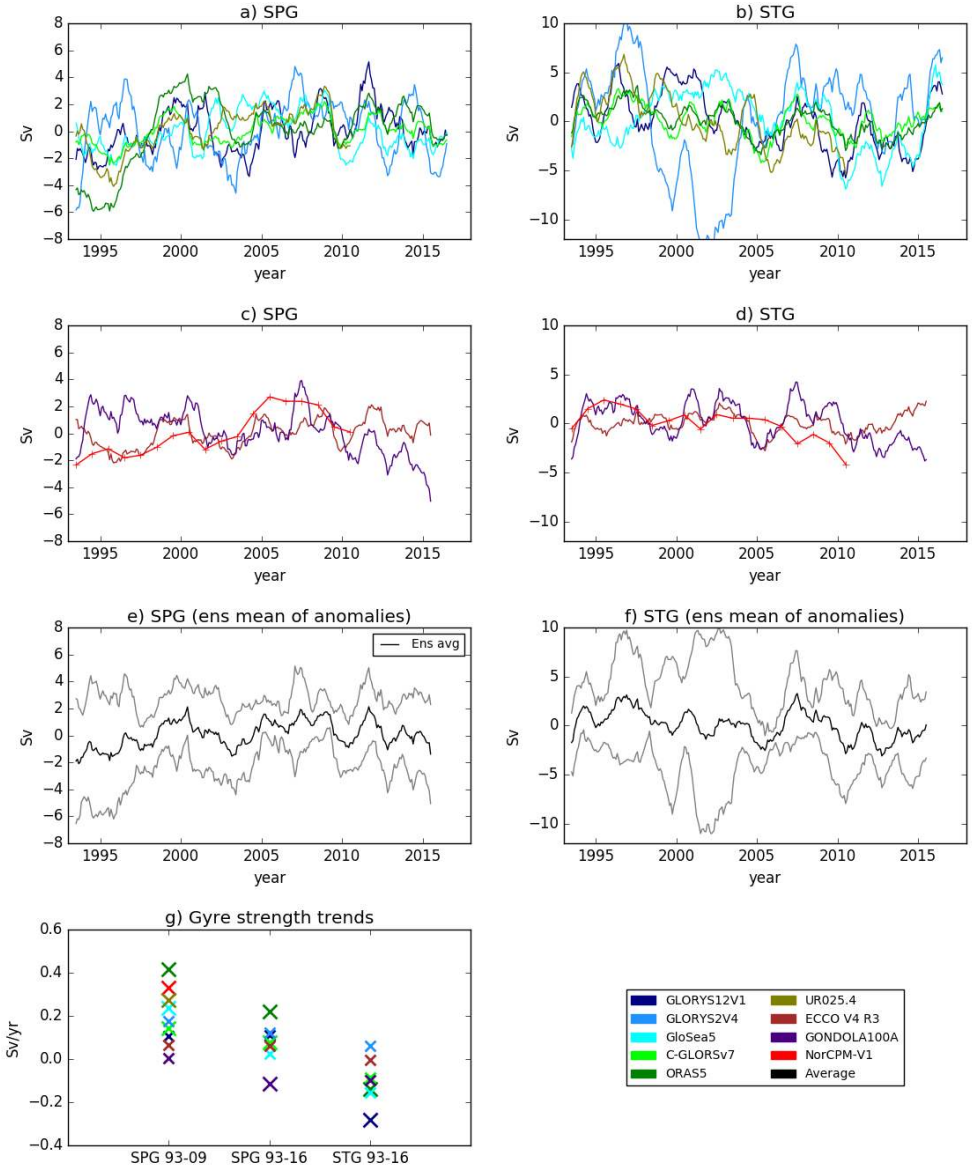

Figure 15. Timeseries of anomalies of gyre strengths (with 12 month running mean). Note that GECCO2 has been omitted from this figure because the variability is much larger than the scales. Individual models for a,c) the SPG (average of the barotropic streamfunction over 60-30^{o}W, 50-60^{o}N) and b,d) the STG (average of the barotropic streamfunction over 80-50^{o}W,25-38^{o}N). e) ensemble mean (black) and 2 x standard deviation (grey) of SPG timeseries. f) As e but for the STG. g) Comparisons of trends across the ensemble. Each cross is a model, with large crosses assessed as significant changes compared to each model timeseries. Black crosses are the changes for the ensemble mean.

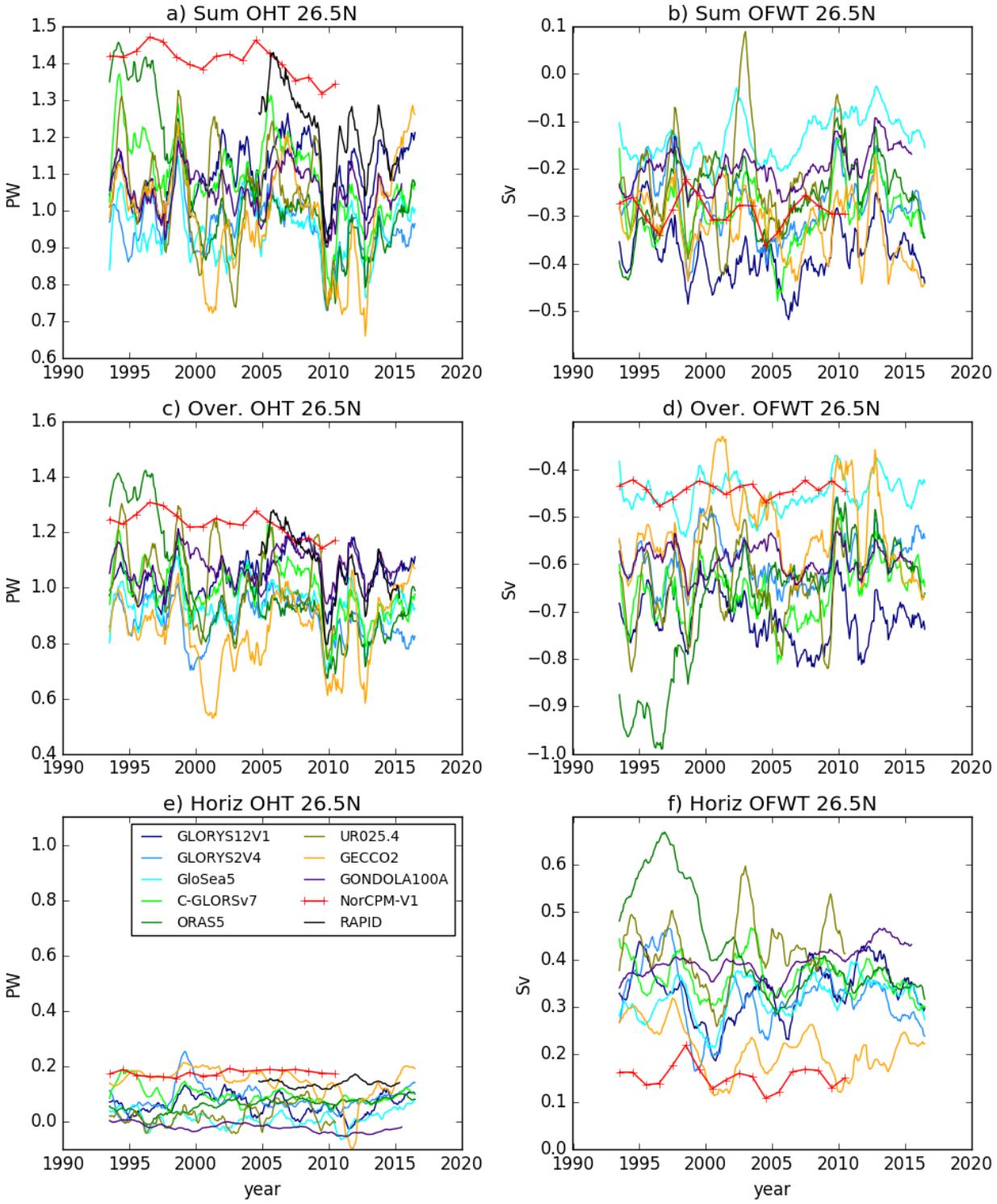

Figure 16. Heat transports (left hand columns) and freshwater transports (right hand columns) at 26.5^{o}N. Shown is the gyre component (bottom), the overturning component (middle) and the sum (top). Note that no throughflow component is included in the sum for the freshwater transport, making it an equivalent freshwater transport referenced to 26.5^{o}N. For equivalent freshwater and transport component definitions see McDonagh et al. (2015).

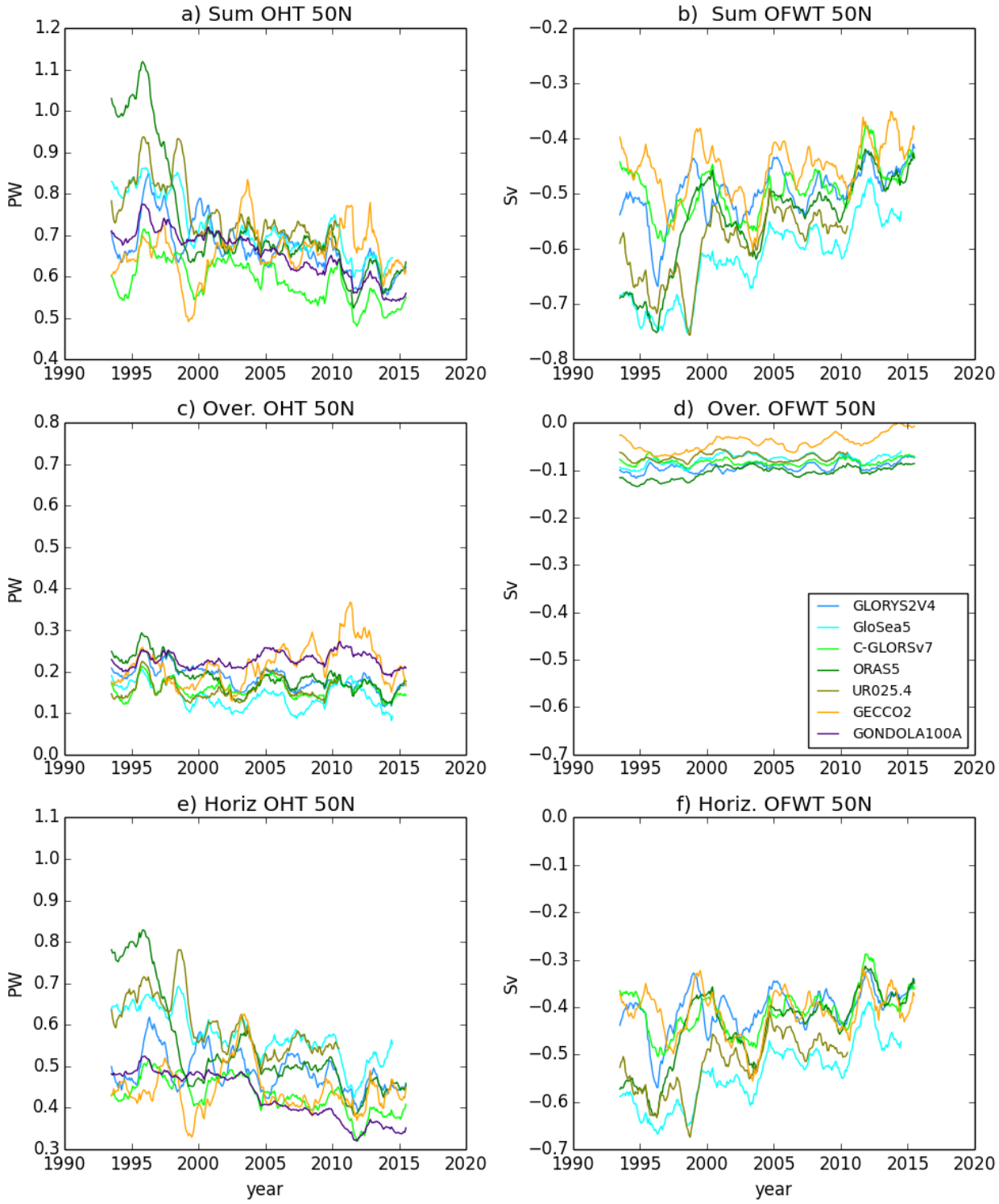

871 **Figure 17.** As Fig 16 but at 50°N.

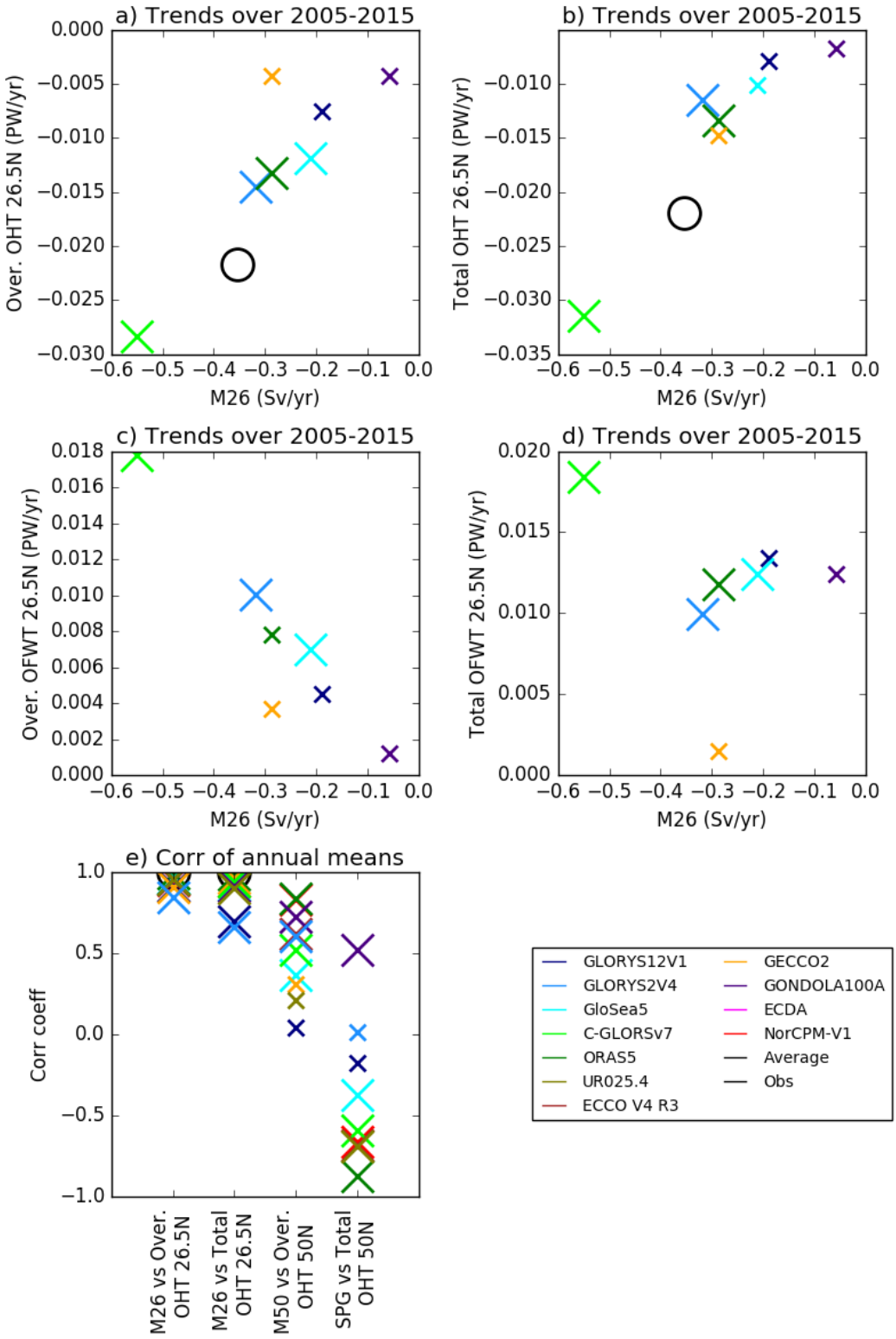

Figure 18. Comparison of the trends of AMOC at 26.5°N (M26) with trends of a) the overturning component of OHT, b) the total heat transport, c) the overturning component of OFWT d) the total component of OFWT. Trends are over 2005-2015 and those reanalyses where both variables have significant trends use a large symbol. Observations from RAPID are shown in black circles. e) Correlations of annual mean timeseries of M26 and M50 with the overturning and total components of heat transport. Large crosses show significant relationships.

References

Ba, J., Keenlyside, N. S., Latif, M., Park, W., Ding, H., Lohmann, K., ... Volodin, E. (2014). A multi-model comparison of atlantic multidecadal variability. *Climate Dynamics*, *43*(9), 2333–2348. doi: 10.1007/s00382-014-2056-1

Balmaseda, M. A., Hernandez, F., Storto, A., Palmer, M. D., Alves, O., Shi, L., ... Gaillard, F. (2015). The Ocean Reanalyses Intercomparison Project (ORA-IP). *Journal of Operational Oceanography*, *8*(sup1), s80–s97. doi: 10.1080/1755876x.2015.1022329

Balmaseda, M. A., Smith, G. C., Haines, K., Anderson, D., Palmer, T. N., & Vidard, A. (2007). Historical reconstruction of the Atlantic Meridional Overturning Circulation from the ECMWF operational ocean reanalysis. *Geophys. Res. Lett.*, *34*(23), L23615+. doi: 10.1029/2007gl031645

Blockley, E. W., Martin, M. J., McLaren, A. J., Ryan, A. G., Waters, J., Lea, D. J., ... Storkey, D. (2014). Recent development of the Met Office operational ocean forecasting system: an overview and assessment of the new global FOAM forecasts. *Geoscientific Model Development*, *7*(6), 2613–2638. doi: 10.5194/gmd-7-2613-2014

Boning, C. W., Scheinert, M., Dengg, J., Biastoch, A., & Funk, A. (2006). Decadal variability of subpolar gyre transport and its reverberation in the North Atlantic overturning. *Geophys. Res. Lett.*, *33*, L21S01. doi: 10.1029/2006GL026906

Bryden, H. L., & Imawaki, I. (2001). Ocean transports of heat. In G. Siedler, J. Church, & J. Gould (Eds.), *Ocean circulation and climate* (p. 455-474). San Diego, USA: San Diego Academic Press. doi: 10.1016/S0074-6142(01)80134-0

Cabanes, C., Grouazel, A., von Schuckmann, K., Hamon, M., Turpin, V., Coatanoan, C., ... Le Traon, P. (2013). The CORA dataset: validation and diagnostics of in-situ ocean temperature and salinity measurements. . *Ocean Science*, *9*, 1–18. doi: 10.5194/os-9-1-2013

Caesar, L., Rahmstorf, S., Robinson, A., Feulner, G., & Saba, V. (2018). Observed fingerprint of a weakening Atlantic Ocean overturning circulation. *Nature*, *556*(7700), 191–196. doi: 10.1038/s41586-018-0006-5

Cassou, C., Deser, C., & Alexander, M. A. (2007). Investigating the impact of reemerging sea surface temperature anomalies on the winter atmospheric cir-

culation over the North Atlantic. *Journal of Climate*, *20*(14), 3510-3526. doi: 10.1175/JCLI4202.1

Chang, Y., Zhang, S., Rosati, A., Delworth, T., & Stern, W. (2013). An assessment of oceanic variability for 1960-2010 from the GFDL ensemble coupled data assimilation. *Climate Dynamics*, *40*, 775-803. doi: 10.1007/s00382-012-1412-2

Chevallier, M., Smith, G. C., Dupont, F., Lemieux, J.-F., Forget, G., Fujii, Y., ... Wang, X. (2017). Intercomparison of the arctic sea ice cover in global ocean–sea ice reanalyses from the ora-ip project. *Climate Dynamics*, *49*(3), 1107–1136. doi: 10.1007/s00382-016-2985-y

Collins, M., Knutti, R., Arblaster, J., Dufresne, J. L., Fichefet, T., Friedlingstein, P., ... Wehner, M. (2013). Long-term Climate Change: Projections, Commitments and Irreversibility. In T. F. Stocker et al. (Eds.), *Climate Change 2013: The Physical Science Basis. Contribution of Working Group I to the Fifth Assessment Report of the Intergovernmental Panel on Climate Change.* Cambridge, United Kingdom and New York, NY, USA.: Cambridge University Press. doi: 10.1017/CBO9781107415324.025

Counillon, F., Keenlyside, N., Bethke, I., Wang, Y., Billeau, S., Shen, M. L., & Bentsen, M. (2016). Flow-dependent assimilation of sea surface temperature in isopycnal coordinates with the Norwegian Climate Prediction Model. *Tellus A: Dynamic Meteorology and Oceanography*, *68*(1), 32437. doi: 10.3402/tellusa.v68.32437

Cunningham, S. A., Roberts, C. D., Frajka-Williams, E., Johns, W. E., Hobbs, W., Palmer, M. D., ... McCarthy, G. (2013). Atlantic Meridional Overturning Circulation slowdown cooled the subtropical ocean. *Geophys. Res. Lett.*, *40*(23), 2013GL058464+. doi: 10.1002/2013gl058464

Danabasoglu, G., Yeager, S. G., Bailey, D., Behrens, E., Bentsen, M., Bi, D., ... Wang, Q. (2014). North Atlantic simulations in Coordinated Ocean-ice Reference Experiments phase II (CORE-II). Part I: Mean states. *Ocean Modelling*, *73*, 76 - 107. doi: https://doi.org/10.1016/j.ocemod.2013.10.005

Danabasoglu, G., Yeager, S. G., Kim, W. M., Behrens, E., Bentsen, M., Bi, D., ... Yashayaev, I. (2016). North Atlantic simulations in Coordinated Ocean-ice Reference Experiments phase II (CORE-II). Part II: Inter-annual to decadal variability. *Ocean Modelling*, *97*, 65–90. doi: 10.1016/j.ocemod.2015.11.007

de Boyer-Montegut, C., Madec, G., Fischer, A. S., Lazar, A., & Iudicone, D. (2004). Mixed layer depth over the global ocean: An examination of profile data and a profile-based climatology. *Journal of Geophysical Research: Oceans*, *109*(C12). doi: 10.1029/2004JC002378

Deshayes, J., & Frankignoul, C. (2008). Simulated variability of the circulation in the North Atlantic from 1953 to 2003. *Journal of Climate*, *21*(19), 4919-4933. doi: 10.1175/2008JCLI1882.1

Duchez, A., Frajka-Williams, E., Josey, S. A., Evans, D. G., Grist, J. P., Marsh, R., ... Hirschi, J. J.-M. (2016). Drivers of exceptionally cold North Atlantic Ocean temperatures and their link to the 2015 European heat wave. *Environmental Research Letters*, *11*(7), 074004. doi: 10.1088/1748-9326/11/7/074004

Dunstone, N., Smith, D., Scaife, A., Hermanson, L., Fereday, D., O'Reilly, C., ... Belcher, S. (2018). Skilful seasonal predictions of summer European rainfall. *Geophysical Research Letters*, *45*(7), 3246-3254. doi: 10.1002/2017GL076337

Eden, C., & Willebrand, J. (2001). Mechanism of Interannual to Decadal Variability of the North Atlantic Circulation. *J. Climate*, *14*(10), 2266–2280. doi: 10.1175/1520-0442

Evans, D. G., Toole, J., Forget, G., Zika, J. D., Naveira Garabato, A. C., Nurser, A. J. G., & Yu, L. (2017). Recent wind-driven variability in Atlantic water mass distribution and meridional overturning circulation. *Journal of Physical Oceanography*, *47*(3), 633-647. doi: 10.1175/JPO-D-16-0089.1

Ferry, N., Parent, L., Garric, G., Bricaud, C., Testut, C.-E., Le Galloudec, O., ... Zawadzki, L. (2012). GLORYS2V1 global ocean reanalysis of the altimetric era (1992-2009) at mesoscale. *Mercator Quarterly Newsletter.*, *44*(44), 29-39.

Forget, G. (2010). Mapping ocean observations in a dynamical framework: A 2004-06 ocean atlas. *Journal of Physical Oceanography*, *40*(6), 1201-1221. doi: 10.1175/2009JPO4043.1

Forget, G., Campin, J.-M., Heimbach, P., Hill, C. N., Ponte, R. M., & Wunsch, C. (2015). ECCO Version 4: an integrated framework for non-linear inverse modeling and global ocean state estimation. *Geoscientific Model Development*, *8*, 3071-3104.

Forget, G., & Ponte, R. (2015). The partition of regional sea level variability. *Progress in Oceanography*, *137*, 173–195.

Foukal, N. P., & Lozier, M. S. (2017). Assessing variability in the size and strength of the North Atlantic subpolar gyre. *Journal of Geophysical Research: Oceans*, *122*(8), 6295-6308. doi: 10.1002/2017JC012798

Fukumori, I., Wang, O., Fenty, I., Forget, G., Heimbach, P., & Ponte, R. M. (2017). *ECCO Version 4 Release 3* (Tech. Rep.). doi: 1721.1/110380

Ganachaud, A., & Wunsch, C. (2003). Large-scale ocean heat and freshwater transports during the World Ocean Circulation Experiment. *Journal of Climate*, *16*(4), 696-705. doi: '10.1175/1520-0442(2003)016⟨0696:LSOHAF⟩2.0.CO;2'

Gent, P. R., & McWilliams, J. C. (1990). Isopycnal mixing in ocean circulation models. *J. Phys. Oceanogr*, *20*, 150–155.

Good, S. A., Martin, M. J., & Rayner, N. A. (2013). EN4: Quality controlled ocean temperature and salinity profiles and monthly objective analyses with uncertainty estimates. *Journal of Geophysical Research*, *118*, 6704–6716.

Grist, J., Josey, S., Jacobs, Z., Marsh, R., Sinha, B., & Van Sebille, E. (2016). Extreme air-sea interaction over the North Atlantic subpolar gyre during the winter of 2013-2014 and its sub-surface legacy. *Climate Dynamics*, *46*(11-12), 4027–4045. doi: 10.1007/s00382-015-2819-3

Häkkinen, S., & Rhines, P. B. (2004). Decline of Subpolar North Atlantic Circulation During the 1990s. *Science*, *304*(5670), 555–559. doi: 10.1126/science.1094917

Hatun, H., & Chafik, L. (2018). On the recent ambiguity of the North Atlantic subpolar gyre index. *Journal of Geophysical Research: Oceans*, *123,*, 5072ž0135076. (https: / / doi. org / 10. 1029 / 2018 JC 014101) doi: 10.1029/2018JC014101

Hermanson, L., Eade, R., Robinson, N. H., Dunstone, N. J., Andrews, M. B., Knight, J. R., ... Smith, D. M. (2014). Forecast cooling of the Atlantic subpolar gyre and associated impacts. *Geophys. Res. Lett.*, *41*(14), 2014GL060420+. doi: 10.1002/2014gl060420

Heuzé, C. (2017). North Atlantic deep water formation and AMOC in CMIP5 models. *Ocean Science*, *13*(4), 609–622. doi: 10.5194/os-13-609-2017

Jackson, L. C., Peterson, K. A., Roberts, C. D., & Wood, R. A. (2016). Recent slowing of Atlantic overturning circulation as a recovery from earlier strengthening. *Nature Geosci*, *9*, 518–522. doi: 10.1038/ngeo2715

1037 Johns, W. E., Baringer, M. O., Beal, L. M., Cunningham, S. A., Kanzow, T., Bry-
1038 den, H. L., ... Curry, R. (2011). Continuous, array-based estimates of Atlantic
1039 Ocean heat transport at 26.5n. *Journal of Climate*, *24*(10), 2429-2449. doi:
1040 10.1175/2010JCLI3997.1

1041 Josey, S. A., Hirschi, J. J.-M., Sinha, B., Duchez, A., Grist, J. P., & Marsh, R.
1042 (2018). The recent Atlantic cold anomaly: Causes, consequences, and related
1043 phenomena. *Annual Review of Marine Science*, *10*(1), 475-501. (PMID:
1044 28934597) doi: 10.1146/annurev-marine-121916-063102

1045 Karspeck, A. R., Stammer, D., Köhl, A., Danabasoglu, G., Balmaseda, M., Smith,
1046 D. M., ... Rosati, A. (2017). Comparison of the atlantic meridional over-
1047 turning circulation between 1960 and 2007 in six ocean reanalysis products.
1048 *Climate Dynamics*, *49*(3), 957–982. doi: 10.1007/s00382-015-2787-7

1049 Knight, J. R., Allan, R. J., Folland, C. K., Vellinga, M., & Mann, M. E. (2005).
1050 A signature of persistent natural thermohaline circulation cycles in observed
1051 climate. *Geophys. Res. Lett*, *32*. doi: 10.1029/2005GL024233

1052 Kohl, A. (2015). Evaluation of the GECCO2 ocean synthesis: transports of volume,
1053 heat and freshwater in the Atlantic. *Quarterly Journal of the Royal Meteoro-*
1054 *logical Society*, *141*, 166-181.

1055 Lellouche, J.-M., Greiner, E., Le Galloudec, O., Garric, G., Regnier, C., Drevillon,
1056 M., ... Le Traon, P.-Y. (2018). Recent updates to the Copernicus Marine
1057 Service global ocean monitoring and forecasting real-time 1/12 high-resolution
1058 system. *Ocean Science*, *14*, 1093-1126. doi: 10.5194/os-14-1093-2018

1059 Lohmann, K., Drange, H., & Bentsen, M. (2009). A possible mechanism for the
1060 strong weakening of the North Atlantic subpolar gyre in the mid-1990s. *Geo-*
1061 *phys. Res. Lett*, *36*, L15602. doi: 10.1029/2009GL039166.

1062 Lozier, M. S., Bacon, S., Bower, A. S., Cunningham, S. A., Femke de Jong, M., de
1063 Steur, L., ... Zika, J. D. (2017). Overturning in the Subpolar North At-
1064 lantic Program: a new international ocean observing system. *Bulletin of the*
1065 *American Meteorological Society*, *98*, 737–752.

1066 Lozier, M. S., Li, F., Bacon, S., Bahr, F., Bower, A. S., Cunningham, S. A., ...
1067 Zhao, J. (2019). A sea change in our view of overturning in the subpolar North
1068 Atlantic. *Science*, *363*(6426), 516–521. doi: 10.1126/science.aau6592

1069 Lübbecke, J., Rodr iguez-Fonseca, B., Richter, I., Mart in-Rey, M., Losada, T., Polo,

I., & Keenlyside, N. (2018). Equatorial Atlantic variability - modes, mechanisms, and global teleconnections. *Wiley Interdisciplinary Reviews: Climate Change*, *9*, e527. doi: 10.1002/wcc.527

Lumpkin, R., & Speer, K. (2007). Global ocean meridional overturning. *Journal of Physical Oceanography*, *37*(10), 2550-2562. doi: 10.1175/JPO3130.1

MacLachlan, C., Arribas, A., Peterson, K. A., Maidens, A., Fereday, D., Scaife, A. A., ... Madec, G. (2015). Global Seasonal forecast system version 5 (GloSea5): a high-resolution seasonal forecast system. *Q. J.R.Meteorol. Soc.*, *141*, 1072-1084.

Masina, S., Storto, A., Ferry, N., Valdivieso, M., Haines, K., Balmaseda, M., ... Parent, L. (2017). An ensemble of eddy-permitting global ocean reanalyses from the MyOcean project. *Climate Dynamics*, *49*(3), 813–841. doi: 10.1007/s00382-015-2728-5

McCarthy, G. D., Frajka-Williams, E., Johns, W. E., Baringer, M. O., Meinen, C. S., Bryden, H. L., ... Cunningham, S. A. (2012). Observed interannual variability of the Atlantic meridional overturning circulation at 26.5N. *Geophys. Res. Lett.*, *39*(19), L19609+. doi: 10.1029/2012gl052933

McCarthy, G. D., Smeed, D. A., Johns, W. E., Frajka-Williams, E., Moat, B. I., Rayner, D., ... Bryden, H. L. (2015). Measuring the Atlantic Meridional Overturning Circulation at 26N. *Progress in Oceanography*, *130*, 91–111. doi: 10.1016/j.pocean.2014.10.006

McDonagh, E. L., King, B. A., Bryden, H. L., Courtois, P., Szuts, Z., Baringer, M., ... McCarthy, G. (2015). Continuous estimate of Atlantic oceanic freshwater flux at 26.5N. *Journal of Climate*, *28*(22), 8888–8906. doi: 10.1175/jcli-d-14-00519.1

McDonagh, E. L., McLeod, P., King, B. A., Bryden, H. L., & Valds, S. T. (2010). Circulation, heat, and freshwater transport at 36n in the Atlantic. *Journal of Physical Oceanography*, *40*(12), 2661-2678. doi: 10.1175/2010JPO4176.1

Menary, M. B., & Hermanson, L. (2018). Limits on determining the skill of North Atlantic Ocean decadal predictions. *Nature Communications*, *9*(1), 1694–. doi: 10.1038/s41467-018-04043-9

Menary, M. B., Hermanson, L., & Dunstone, N. J. (2016). The impact of labrador sea temperature and salinity variability on density and the subpolar amoc in

a decadal prediction system. *Geophys. Res. Lett.*, *43*, 12,217-12,227. doi: 10.1002/2016GL070906

Menary, M. B., Hodson, D. L. R., Robson, J. I., Sutton, R. T., Wood, R. A., & Hunt, J. A. (2015). Exploring the impact of CMIP5 model biases on the simulation of North Atlantic decadal variability. *Geophysical Research Letters*, *42*(14), 5926-5934. doi: 10.1002/2015GL064360

Mignac, D., Ferreira, D., & Haines, K. (2019). Decoupled freshwater transport and meridional overturning in the South Atlantic. *Geophysical Research Letters*, *46*. doi: 10.1029/2018GL081328

Msadek, R., Johns, W. E., Yeager, S. G., Danabasoglu, G., Delworth, T. L., & Rosati, A. (2013). The Atlantic Meridional Heat Transport at 26.5N and Its Relationship with the MOC in the RAPID Array and the GFDL and NCAR Coupled Models. *Journal of Climate*, *26*(12), 4335-4356. doi: 10.1175/JCLI-D-12-00081.1

Palmer, M. D., & Haines, K. (2009). Estimating oceanic heat content change using isotherms. *Journal of Climate*, *22*(19), 4953-4969. doi: 10.1175/2009JCLI2823.1

Palmer, M. D., Roberts, C. D., Balmaseda, M., Chang, Y.-S., Chepurin, G., Ferry, N., ... Xue, Y. (2017). Ocean heat content variability and change in an ensemble of ocean reanalyses. *Climate Dynamics*, *49*(3), 909–930. doi: 10.1007/s00382-015-2801-0

Peings, Y., & Magnusdottir, G. (2014). Forcing of the wintertime atmospheric circulation by the multidecadal fluctuations of the North Atlantic ocean. *Environmental Research Letters*, *9*(3), 034018+. doi: 10.1088/1748-9326/9/3/034018

Piecuch, C. G., Ponte, R. M., Little, C. M., Buckley, M. W., & Fukumori, I. (2017). Mechanisms underlying recent decadal changes in subpolar North Atlantic Ocean heat content. *J. Geophys. Res. Oceans*, *122*, 7181-7197. doi: 10.1002/2017JC012845

Rhein, M., Rintoul, S., Aoki, S., Campos, E., Chambers, D., Feely, R., ... Wang, F. (2013). Observations: Ocean. In T. Stocker et al. (Eds.), *Climate Change 2013: The Physical Science Basis. Contribution of Working Group I to the Fifth Assessment Report of the Intergovernmental Panel on Climate Change* (p. 255-316). Cambridge, United Kingdom and New York, NY, USA: Cam-

bridge University Press. doi: 10.1017/CBO9781107415324.010

Roberts, C. D., Garry, F. K., & Jackson, L. C. (2013b). A Multimodel Study of Sea Surface Temperature and Subsurface Density Fingerprints of the Atlantic Meridional Overturning Circulation. *J. Climate*, *26*(22), 9155–9174. doi: 10.1175/jcli-d-12-00762.1

Roberts, C. D., Waters, J., Peterson, K. A., Palmer, M. D., McCarthy, G. D., Frajka-Williams, E., ... Zuo, H. (2013a). Atmosphere drives recent interannual variability of the Atlantic meridional overturning circulation at 26.5N. *Geophys. Res. Lett.*, *40*(19), 5164–5170. doi: 10.1002/grl.50930

Roberts, M. J., Hewitt, H. T., Hyder, P., Ferreira, D., Josey, S. A., Mizielinski, M., & Shelly, A. (2016). Impact of ocean resolution on coupled airsea fluxes and largescale climate. *Geophysical Research Letters*, *43*, 10,430–10,438.

Robson, J., Hodson, D., Hawkins, E., & Sutton, R. (2014). Atlantic overturning in decline? *Nature Geoscience*, *7*(1), 2–3. doi: 10.1038/ngeo2050

Robson, J., Ortega, P., & Sutton, R. (2016). A reversal of climatic trends in the North Atlantic since 2005. *Nature Geoscience*, *9*(7), 513–517. doi: 10.1038/ngeo2727

Robson, J., Sutton, R., Lohmann, K., Smith, D., & Palmer, M. D. (2012). Causes of the Rapid Warming of the North Atlantic Ocean in the Mid-1990s. *J. Climate*, *25*(12), 4116–4134. doi: 10.1175/jcli-d-11-00443.1

Robson, J., Sutton, R. T., Archibald, A., & et al. (2018). Recent multivariate changes in the North Atlantic climate system, with a focus on 2005- 2016. *Int J Climatol*, *38*, 5050-5076. doi: 10.1002/joc.5815

Shi, L., Alves, O., Wedd, R., Balmaseda, M. A., Chang, Y., Chepurin, G., ... Yin, Y. (2017). "an assessment of upper ocean salinity content from the ocean reanalyses inter-comparison project (ora-ip)". *Climate Dynamics*, *49*(3), 1009–1029. doi: 10.1007/s00382-015-2868-7

Smeed, D. A., Josey, S. A., Beaulieu, C., Johns, W. E., Moat, B. I., Frajka-Williams, E., ... McCarthy, G. D. (2018). The North Atlantic Ocean Is in a State of Reduced Overturning. *Geophys. Res. Lett.*, *45*, 2017GL076350+. doi: 10.1002/2017gl076350

Smeed, D. A., McCarthy, G., Rayner, D., Moat, B., Johns, W., Baringer, M., & Meinen, C. (2017). *Atlantic meridional overturning circulation observed by*

the RAPID-MOCHA-WBTS (RAPID-Meridional Overturning Circulation and Heatflux Array-Western Boundary Time Series) array at 26N from 2004 to 2017. Natural Environment Research Council, UK.: British Oceanographic Data Centre. Retrieved from `https://www.rapid.ac.uk/rapidmoc/rapid_data/datadl.php` doi: 10.5285/5acfd143-1104-7b58-e053-6c86abc0d94b

Smith, D., Eade, R., Dunstone, N., Fereday, D., Murphy, J., Pohlman, H., & Scaife, A. (2010). Skillful multi-year predictions of Atlantic hurricane frequency. *Nature Geoscience*, *3*, 846-849. doi: doi:10.1038/NGEO1004

Stepanov, V. N., Iovino, D., Masina, S., Storto, A., & Cipollone, A. (2016). Observed and simulated variability of the Atlantic Meridional Overturning Circulation at 41N. *Journal of Marine Systems*, *164*, 42–52. doi: 10.1016/j.jmarsys.2016.08.004

Storto, A., Alvera-Azcarate, A., Balmesada, M. A., Barth, A., Chevallier, M., Counillon, F., ... Zuo, H. (2019). Ocean reanalyses: recent advances and unsolved challenges. *Frontiers in Marine Science*, *6*, 418.

Storto, A., & Masina, S. (2016). C-GLORSv5: an improved multipurpose global ocean eddy-permitting physical reanalysis. *Earth Syst. Sci. Data*, *8*, 679-696. doi: 10.5194/essd-8-679-2016

Storto, A., Masina, S., Balmaseda, M., Guinehut, S., Xue, Y., Szekely, T., ... Wang, X. (2017). Steric sea level variability (1993–2010) in an ensemble of ocean reanalyses and objective analyses. *Climate Dynamics*, *49*(3), 709–729. doi: 10.1007/s00382-015-2554-9

Storto, A., Masina, S., & Navarra, A. (2016). Evaluation of the CMCC eddy-permitting global ocean physical reanalysis system (C-GLORS, 1982-2012) and its assimilation components. *Q.J.R. Meteorol. Soc.*, *142*, 738-758. doi: 10.1002/qj.2673

Storto, A., Masina, S., Simoncelli, S., Iovino, D., Cipollone, A., Drevillon, M., ... Peterson, K. A. (2018). The added value of the multi-system spread information for ocean heat content and steric sea level investigations in the cmems grep ensemble reanalysis product. *Climate Dynamics*. doi: 10.1007/s00382-018-4585-5

Sutton, R. T., & Dong, B. (2012). Atlantic Ocean influence on a shift in European climate in the 1990s. *Nature Geosci*, *5*(11), 788–792. doi: 10.1038/ngeo1595

Sutton, R. T., McCarthy, G. D., Robson, J., Sinha, B., Archibald, A. T., & Gray, L. J. (2018). Atlantic multidecadal variability and the u.k. acsis program. *Bulletin of the American Meteorological Society*, *99*(2), 415-425. doi: 10.1175/BAMS-D-16-0266.1

Talley, L. D. (2003). Shallow, intermediate, and deep overturning components of the global heat budget. *Journal of Physical Oceanography*, *33*(3), 530-560. doi: {10.1175/1520-0485(2003)033⟨0530:SIADOC⟩2.0.CO;2}

Talley, L. D. (2008). Freshwater transport estimates and the global overturning circulation: Shallow, deep and throughflow components. *Progress in Oceanography*, *78*(4), 257 - 303. doi: 10.1016/j.pocean.2008.05.001

Tett, S. F. B., Sherwin, T. J., Shravat, A., & Browne, O. (2014). How Much Has the North Atlantic Ocean Overturning Circulation Changed in the Last 50 Years? *J. Climate*, *27*(16), 6325–6342. doi: 10.1175/jcli-d-12-00095.1

Thornalley, D. J. R., Oppo, D. W., Ortega, P., Robson, J. I., Brierley, C. M., Davis, R., ... Keigwin, L. D. (2018). Anomalously weak Labrador Sea convection and Atlantic overturning during the past 150 years. *Nature*, *556*(7700), 227–230. doi: 10.1038/s41586-018-0007-4

Tietsche, S., Balmaseda, M. A., Zuo, H., & Mogensen, K. (2017). Arctic sea ice in the global eddy-permitting ocean reanalysis orap5. *Climate Dynamics*, *49*(3), 775–789. doi: 10.1007/s00382-015-2673-3

Toyoda, T., Fujii, Y., Kuragano, T., Kamachi, M., Ishikawa, Y., Masuda, S., ... Lee, T. (2017a). Intercomparison and validation of the mixed layer depth fields of global ocean syntheses. *Climate Dynamics*, *49*(3), 753–773. doi: 10.1007/s00382-015-2637-7

Toyoda, T., Fujii, Y., Kuragano, T., Kosugi, N., Sasano, D., Kamachi, M., ... Balmaseda, M. (2017b). Interannual-decadal variability of wintertime mixed layer depths in the north pacific detected by an ensemble of ocean syntheses. *Climate Dynamics*, *49*(3), 891–907. doi: 10.1007/s00382-015-2762-3

Toyoda, T., Fujii, Y., Yasuda, T., Usui, N., Ogawa, K., Kuragano, T., ... Kamachi, M. (2016). Data assimilation of sea ice concentration into a global ocean-sea ice model with corrections for atmospheric forcing and ocean temperature fields. *J Oceanogr*, *72*, 235-262. doi: 10.1007/s10872-015-0326-0

Treguier, A. M., Deshayes, J., Lique, C., Dussin, R., & Molines, J. M. (2012). Eddy

contributions to the meridional transport of salt in the North Atlantic. *Journal of Geophysical Research: Oceans*, *117*, C05010. doi: 10.1029/2012JC007927

Uotila, P., Goosse, H., Haines, K., Chevallier, M., Barthélemy, A., Bricaud, C., ... Zhang, Z. (2018). An assessment of ten ocean reanalyses in the polar regions. *Climate Dynamics*. doi: 10.1007/s00382-018-4242-z

Vage, K., Pickart, R. S., Thierry, V., Reverdin, G., Lee, C. M., Petrie, B., ... Ribergaard, M. H. (2008). Surprising return of deep convection to the subpolar North Atlantic Ocean in winter 2007-2008. *Nature Geoscience*, *2*, 67–.

Valdivieso, M., Haines, K., Balmaseda, M., Chang, Y.-S., Drevillon, M., Ferry, N., ... Andrew Peterson, K. (2017). An assessment of air-sea heat fluxes from ocean and coupled reanalyses. *Climate Dynamics*, *49*(3), 983–1008. doi: 10.1007/s00382-015-2843-3

Valdivieso, M., Haines, K., Zuo, H., & Lea, D. (2014). Freshwater and heat transports from global ocean synthesis. *J. Geophys. Res. Oceans*, *119*(1), 394–409. doi: 10.1002/2013jc009357

von Schuckmann, K., & et al. (2018). Copernicus Marine Service Ocean State Report 2. *Journal of Operational Oceanography*, *11:sup1*, S1-S142. doi: 10.1080/1755876X.2018.1489208

Wang, Y., Counillon, F., Bethke, I., Keenlyside, N., Bocquet, M., & l. Shen, M. (2017). Optimising assimilation of hydrographic profiles into isopycnal ocean models with ensemble data assimilation. *Ocean Modelling*, *114*, 3344. doi: 10.1016/j.ocemod.2017.04.007

Wijffels, S. E. (2001). Ocean transport of fresh water. In G. Siedler, J. Church, & J. Gould (Eds.), *Ocean circulation and climate* (p. 475-488). San Diego, USA: San Diego Academic Press. doi: 10.1016/S0074-6142(01)80135-2

Williams, R. G., Roussenov, V., Smith, D., & Lozier, M. S. (2014). Decadal Evolution of Ocean Thermal Anomalies in the North Atlantic: The Effects of Ekman, Overturning, and Horizontal Transport. *Journal of Climate*, *27*(2), 698-719. doi: 10.1175/JCLI-D-12-00234.1

Yang, C., Masina, S., Bellucci, A., & Storto, A. (2016). The Rapid Warming of the North Atlantic Ocean in the Mid-1990s in an Eddy-Permitting Ocean Reanalysis (1982-2013). *J. Climate*, *29*(15), 5417–5430. doi: 10.1175/jcli-d-15-0438.1

Yashayaev, I., & Loder, J. W. (2017). Further intensification of deep convection in

1268 the Labrador Sea in 2016. *Geophys. Res. Lett.*, *44*(3), 2016GL071668+. doi: 10
1269 .1002/2016gl071668

1270 Yeager, S. (2015). Topographic coupling of the Atlantic overturning and gyre circu-
1271 lations. *Journal of Physical Oceanography*, *45*(5), 1258-1284. doi: 10.1175/JPO
1272 -D-14-0100.1

1273 Yeager, S., & Danabasoglu, G. (2014). The Origins of Late-Twentieth-Century Vari-
1274 ations in the Large-Scale North Atlantic Circulation. *J. Climate*, *27*(9), 3222–
1275 3247. doi: 10.1175/jcli-d-13-00125.1

1276 Zhang, R., & Delworth, T. L. (2006). Impact of Atlantic multidecadal oscillations on
1277 India/Sahel rainfall and Atlantic hurricanes. *Geophys. Res. Lett.*, *33*, L17712.
1278 doi: 10.1029/2006GL026267.

1279 Zhang, S., Harrison, M. J., Rosati, A., & Wittenberg, A. T. (2007). System design
1280 and evaluation of coupled ensemble data assimilation for global oceanic climate
1281 studies. *Monthly Weather Review*, *135*, 3541-3564. doi: 10.1175/MWR3466.1

1282 Zuo, H., A, B. M., Tietsche, S., Mogensen, K., & Mayer, M. (2019). The ECMWF
1283 operational ensemble reanalysis-analysis system for ocean and sea-ice: a
1284 description of the system and assessment. *Ocean Sci.*, *15*, 779–808. doi:
1285 10.5194/os-15-779-2019